AD-A230 502

DEPARTMENT OF THE AIR FORCE

AIR UNIVERSITY

AIR FORCE INSTITUTE OF TECHNOLOGY

Wright-Patterson Air Force Base, Ohio

91 1 3 136

AFIT/GE/ENG/90D-54

RADAR IMAGE PROCESSING FOR
THE AFIT ANECHOIC CHAMBER

Thesis

Brian K. Sanders, Captain, USAF

AFIT/GE/ENG/90D-54

Approved for public release; distribution unlimited

RADAR IMAGE PROCESSING FOR

THE AFIT ANECHOIC CHAMBER

Thesis

Presented to the Faculty of the School of Engineering

of the Air Force Institute of Technology

Air University

In Partial Fulfillment of the Requirements of the Degree of

Master of Science in Electrical Engineering

Brian K. Sanders, B.S.

Captain, USAF

December 1990

Accession For		
NTIS GRA&I		☒
DTIC TAB		☐
Unannounced		☐
Justification		
By		
Distribution/		
Availability Codes		
Dist	Avail and/or Special	
A-1		

Acknowledgements

Table of Contents

List of Figures

Abstract

The purpose of this study was to begin development of an Inverse Synthetic Aperture Radar imaging capability for the AFIT anechoic chamber. This began with an evaluation of the capabilities and limitations of the existing radar system and the chamber itself for this application. Then, after deciding on the image processing approach, software had to be written to collect the data necessary for image processing. This constituted the majority of this study, and resulted in a versatile, user-friendly program that automates the process of collecting data for high-resolution radar images. The program checks that the data to be collected will lead to a valid radar cross-section (RCS) image, but will allow data collection for general radar images. Finally, the image processing software was begun. This made use of commercially available software packages called PC-MATLAB and PRO-MATLAB. Further work is needed on the image processing software to generate calibrated images, and to perform image focusing.

RADAR IMAGE PROCESSING FOR

THE AFIT ANECHOIC CHAMBER

I. Introduction

1.1 Prologue

This thesis presents the development of an Inverse Synthetic Aperture Radar (ISAR) imaging system for the Air Force Institute of Technology (AFIT) anechoic chamber. The existing radar hardware and portions of the system software are used in the development of this system. The major tasks accomplished during this effort include:

a. The existing radar system and the anechoic chamber were evaluated for their capabilities and limitations in this application.

b. Image data was collected for a single test target through repeated use of the existing frequency response software at several

azimuth angles. An image was produced using PC-MATLAB software. This work was used as a demonstration of present capabilities.

c. Existing software for data collection was modified to collect the array of data necessary for the production of radar images.

d. Software for transferring data files from the Hewlett-Packard computer (which controls the radar system) to an IBM compatible computer was revised to accommodate the data array.

e. Limited capability data processing software was written for IBM compatible computer systems, either personal computers (PCs) or a VAX system, using PC-MATLAB software.

f. Image data was collected and processed to validate the capability.

The remainder of this chapter presents an introduction to radar imaging concepts followed by a summary of the history and current work in this field. Next the thesis problem is addressed along with the scope of this work and the general approach for solving the problem. Finally, a synopsis of the balance of this report is presented.

1.2 Radar Imaging Concepts

The classic use of radar has been to determine a target's range, azimuthal position, and radial velocity. Recently, radars have also been used in the two related fields of terrain mapping and target imaging.

When a radar is used for range estimation, a narrow pulse of energy is transmitted in the direction of the target. The target range is

determined by measuring the two way time delay of the reflected pulse and multiplying this time by the known propagation velocity. If the transmitted pulse is sufficiently narrow it is possible to distinguish individual target features in the range direction (3:371-374; 10:9-12; 21:37-39).

The simplest radar for measuring a target's radial velocity is a continuous wave (CW) radar. A target with a velocity component in the radial direction of the radar will reflect the CW signal with some frequency shift. The radial velocity of the target is calculated from the measured frequency shift and the known signal propagation velocity (17:70-81).

A rudimentary method of measuring a target's azimuthal position is to transmit the electromagnetic energy in a narrow beam that is pointed directly at the target. The target's azimuth is measured from the antenna's pointing direction. Using this method requires that the radar beam be no wider than the azimuth resolution desired. For a radar operating at a range R, having a carrier frequency ω_c, and with an antenna aperture size D the azimuthal resolution will be given by $R\omega_c/D$. For very fine resolution requirements, a radar operating in the microwave frequencies (10^9 Hz) would need an antenna several thousand feet across. In many applications such an antenna would be completely impractical; however, this gigantic antenna can be synthesized by moving a small antenna and collecting data over a large region in space in a process known as synthetic aperture radar (9:1; 10:20).

Synthetic aperture radar (SAR) is most commonly known as a means of obtaining high resolution terrain maps. By coherently processing the backscattered phase history of a target, an effective antenna aperture many times larger than the physical antenna is produced. The large effective aperture produces a correspondingly narrow beamwidth and consequentially provides fine azimuthal resolution. A subset of SAR that achieves even finer resolutions is spotlight mode SAR. In spotlight mode SAR, the antenna is continuously steered to point at a specific patch of terrain during the aircraft's flight. Thus, the patch of terrain is viewed from many different aspect angles. The coherent processing of these different views will produce much finer resolution than is possible from a single observation angle (3:386-387).

Inverse synthetic aperture radar (ISAR) is a special case of spotlight mode SAR. In this application the antenna is fixed and the target is rotated about a central axis. Whether the radar moves about the target, as in spotlight mode SAR, or the target rotates relative to a fixed antenna, the results are the same (10:50; 21:274-275).

Radar imaging combines the fine range resolutions inherent in narrow pulse, wide bandwidth signals with the fine azimuthal (cross-range) resolutions obtained by the coherent processing of many aspect angles to produce a two-dimensional image of a target. Due to the high resolutions available in these processes, the target can be reduced to a collection of various scattering centers. At sufficiently high frequencies (target dimensions on the order of ten wavelengths), these scattering centers act independently of each other. Therefore, more

information is available on each of the scatterers that compose the target (3:371).

1.3 *History of Radar Imaging*

The history of imaging radars is quite lengthy; Ausherman (1:366-369) has done a fine job of summarizing the work of several decades, citing 35 articles in his history section alone. Presented here is a synopsis of that work; interested readers are encouraged to refer to the article by Ausherman.

Initial developments in the field of radar imaging started in the early 1950s. Government, primarily military, interest in this technology fueled studies in the area of SAR development with applications being found in terrain mapping, oceanography, and ice studies. In the late 1950s the concept of delay-Doppler was used to produce images of the Moon and later this technique was used to image Venus. In the late 1960s, a technique for imaging rotating objects was developed. The processing technique devised was to Fourier transform the range data followed by distorting the range transform plane to achieve better resolution, and finally a two-dimensional Fourier transform of the distorted data was taken to produce the image. In the 1970s rotating platform work resulted in a more generalized formulation of range-Doppler imaging theory and saw the introduction of the polar-format storage techniques which solve the problem of image smearing associated with the motion of scatterers through resolution cells during data collection.

1.4 Developments in Radar Imaging

Recent research in radar imaging has concentrated on improving resolution capabilities, decreasing processing time, target recognition, and three-dimensional imaging.

Gabriel (4:48-55) presents an application of superresolution techniques as a means for improving the resolution of an image using the same number of data samples as previously collected or producing equal-quality images from fewer data samples.

Halevy (5:53-57) discusses several data processing techniques that should significantly reduce the computer processing time needed to produce images. These techniques allow real time imaging using high speed personal computers.

Target recognition using radar imaging has been and will continue to be of great interest to the military, and much of the work in this area is of a classified nature. Both the Navy and the Air Force have done extensive research in this area, imaging both ships and aircraft of all types. Two sources of open literature in this area are the articles by Prickett (14:340-345) and Steinberg (18:663-669). Prickett presents ISAR techniques applied in imaging ships at sea. Steinberg suggests a method of identifying aircraft based on sectioning the images into various aircraft major assemblies (nose, fuselage, tail, far and near wing).

The advent of increased computing power and greater storage capacity has created the possibilities for the three-dimensional imaging of objects. In producing a two-dimensional image the separation in the

vertical direction of the scattering centers has been collapsed. Thus, any scattering centers that have the same range and cross-range positions but not the same vertical position will be imaged into the same range/cross-range cell. Reedy (16:7-11) and Currie (3:376-403), present a system developed by the Georgia Technical Research Institute that operates at 95 GHz and has a resolution of one foot or greater in all three dimensions. Although limited in capability, the system does demonstrate the potential provided by three-dimensional imaging.

1.5 Problem

The objective of this thesis is to develop an ISAR imaging capability for the AFIT anechoic chamber. The AFIT chamber is used to instruct the Low Observables students in radar scattering characteristics, and as a research tool. Presently, the system measures the radar return versus azimuth angle at a fixed frequency (which presents the data in the standard magnitude versus angle format) and the complex frequency response at a fixed azimuth angle. The frequency response is then used to determine a one-dimensional image known as the bandlimited impulse response or range profile, which presents the data in a magnitude versus time (or range) format.

1.6 Scope

This thesis effort provides the AFIT anechoic chamber with a basic ISAR imaging capability. The imaging system will not be a real-time

system due to computer processing constraints and the necessity of the high speed computer hardware to support real-time processing. Instead, images will be produced by post-processing the data on either a PC or the AFIT VAX computer system. Software for collecting ISAR imaging data will be written for the Hewlett-Packard (HP) based radar system currently installed in the chamber. A data processing program will be written using PC-MATLAB software for either of the two possible post processing systems.

1.7 Approach

The data will be collected using the Hewlett-Packard based radar system installed in the AFIT anechoic chamber. The data will be collected according to the following procedure:

1) The calibration target background will be measured and the values stored. This measurement will be subtracted from the calibration target measurement.

2) The calibration target (sphere) will be measured and the values stored.

3) The target background will be measured and the values stored. This measurement will be subtracted from the target measurement. Due to the necessity of rotating the target through several azimuth degrees to obtain the full data array, all target supports must be azimuthally symmetric.

4) The target will be mounted on its support and the frequency dependent range profile data will be collected at each $\delta\theta$

($\delta\theta$= angular aperture/(# of samples) or the incremental angle moved between each target measurement) point needed to produce the array. Each of these range profiles will be one column in the frequency versus aspect angle array.

After data collection is completed, the array will be transferred via an RS232 cable to a Zenith 248 personal computer. The Z-248 will be used to record the array as an ASCII text file and as the primary post processing system. The AFIT VAX computer system will be considered for use if the image array is too large for the memory restrictions on the Z-248 or if the Z-248 is simply too slow.

For unfocused images (small total look angle, $\Delta\theta$), the image array will be processed in the following manner (10:84-92):

1) Each column and row in the data array will be multiplied by a weighting function (windowing) to reduce the cross-range sidelobes.

2) The array will be padded with zeros to produce a 2^m by 2^n array. This padding allows the use of Fast Fourier Transform (FFT) algorithms in the processing.

3) A two-dimensional IFFT will be applied to the array.

4) The resultant reflectivity distribution map will be displayed on the terminal screen. Hard copy output will be produced on demand.

1.8 Synopsis

This thesis report consists of five chapters. Chapter 2 describes the theory of ISAR imaging to include: range resolution, cross-range resolution, frequency and angle Nyquist sampling criterion, unfocused

imaging restrictions, and image data processing including focusing requirements. Chapter 3 examines the AFIT Anechoic chamber and radar system, and evaluates the use of the system for generating radar images. Chapter 4 presents the data collection and processing software. The results of the system validation phase are presented. Chapter 5 presents the conclusions and recommendations for continued research.

II. Radar Imaging Theory

This chapter presents the theory of imaging radars. As indicated in Chapter 1, imaging radars have many forms and applications. However, all are coherent radars that make use of range/Doppler principles to obtain the desired images. In general these radars use conventional, narrow-pulse, wide bandwidth systems to achieve fine range resolution and use the Doppler frequency gradient generated by the relative motion between the target and the radar to achieve cross-range resolutions finer than the radar beamwidth. This chapter is presented in the following manner: first, the scattering center concept of radar targets is developed; second, the imaging theory is presented, discussing range resolution theory first and cross-range resolution theory second; the third subject is the motion of scattering centers through resolution cells, the restrictions this motion imposes, and the solution to the problem; fourth, a presentation of various author's viewpoints on what constitutes a radar cross section (RCS) image versus what the present technology will allow; the fifth topic is the data processing needed to produce radar images; and finally the chapter ends with a summary of the important points presented in the theory.

2.1 Radar Imaging Concepts

Radars respond to the electromagnetic energy that is scattered when an electromagnetic wave's propagation is disturbed by the presence

of an object. The incident electromagnetic wave will induce a distribution of currents on the object which in turn establish the scattered electromagnetic fields (3:370; 10:1). Understandably, the various components of the object will interact differently with the electromagnetic energy depending on the individual components physical characteristics and orientation to the electromagnetic wave's propagation direction (21:19-21).

A comparison of low resolution radar measurements and high resolution radar measurements will help in explaining the concept of an object being composed of a collection of scattering centers. Figure 2.1 illustrates a low resolution radar illuminating an object composed of discrete scatterers. In radars that have low range resolution the scattered fields produced by the various components of the object are spaced close in time. If the radar also exhibits low azimuth resolution the returns from the components separated in the azimuth direction will be measured simultaneously due to the broad beamwidth. Thus, the backscattered energy received from the object will be the superposition of the phasor components of the field. The object's radar return or radar cross section (RCS) for a narrowband radar can be expressed as

$$\sigma = |\sum_{K=1}^{N} (\sigma_K)^{1/2} \exp(j\phi_K)|^2 \qquad (2.1)$$

where $\phi_K = (4\pi d_K)/\lambda$ is the relative two-way phase path for the Kth scatterer, d_K is the relative range of the Kth scatterer, and σ_K is the RCS (expressed as a complex radar return) of the Kth scatterer.
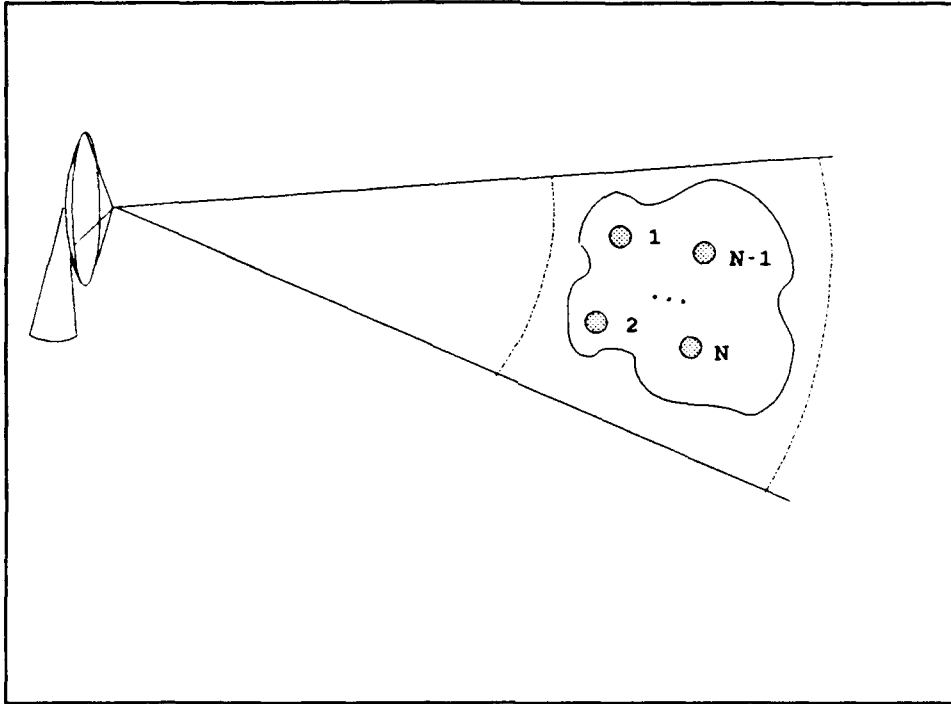
Figure 2.1   Low Resolution Measurement (3:371)

Equation 2.1 is the phasor summation of the echoes received from the individual scatterers.   The important point to note here is that this summation will fluctuate rapidly with changes in the objects's aspect angle, due to the changes in d_K.   Also, small variations in the radar frequency will change the relative phase between the scattering centers resulting in a pronounced effect on the total RCS.   Figure 2.2 shows a radar making a low resolution measurement of a target.   Notice that the radar pulsewidth, τ, and beamwidth, β_{el} x β_{Az}, are such that the entire target is contained in one resolution cell.   Thus, it is impossible for the radar to resolve the individual scatterers that compose the target, and information on those scatterers is lost (3:370; 21:22-23).
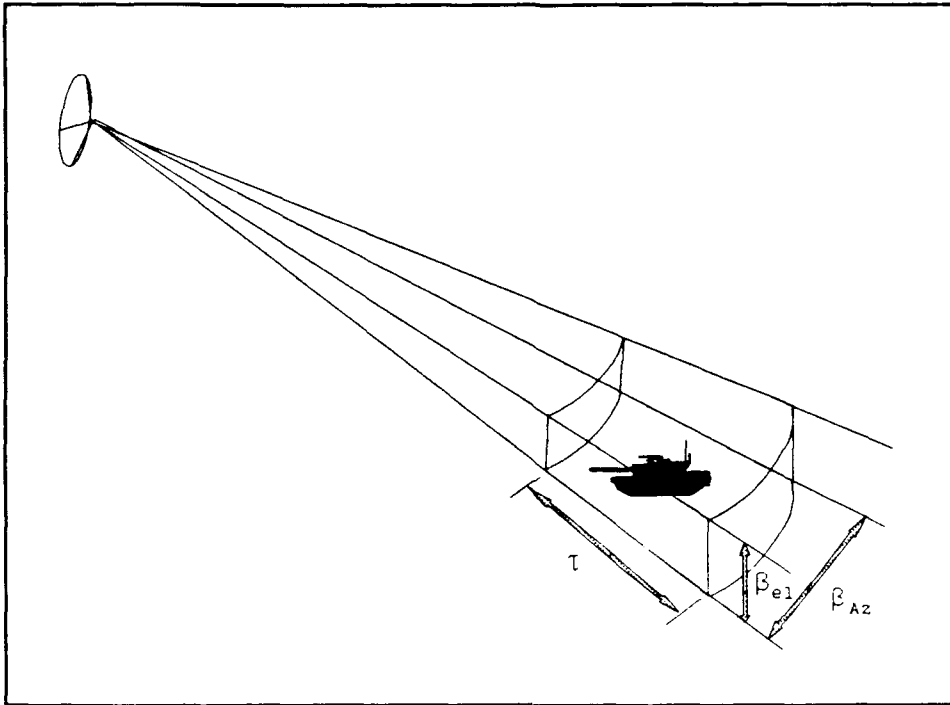
Figure 2.2   Low Resolution RCS Measurement - Total RCS
(3:372)

High resolution measurements have the ability to resolve closely

spaced scattering centers in one or more dimensions.   Figure 2.3

illustrates the three possible dimensions that are available with high

resolution measurements.   In the one-dimensional case, the object is

divided into resolution cells along the radar line-of-sight.   For the

two-dimensional case, the object is divided into resolution cells in

both the range and cross-range directions.   For the three-dimensional

case, the resolution cell takes the shape of a narrow cylinder.   The

measurement is made by performing a raster scan of the object.   This

scanning provides the resolution in the third or elevation dimension

(3:373).

One-dimensional

Object Space

Range Resolution Cell

Two-dimensional

Object Space

Intersection of Down- and Cross-Range Resolution Cells

Three-dimensional

Object Space

Intersection of Down-, Cross-, and Elevation-Range Resolution Cells
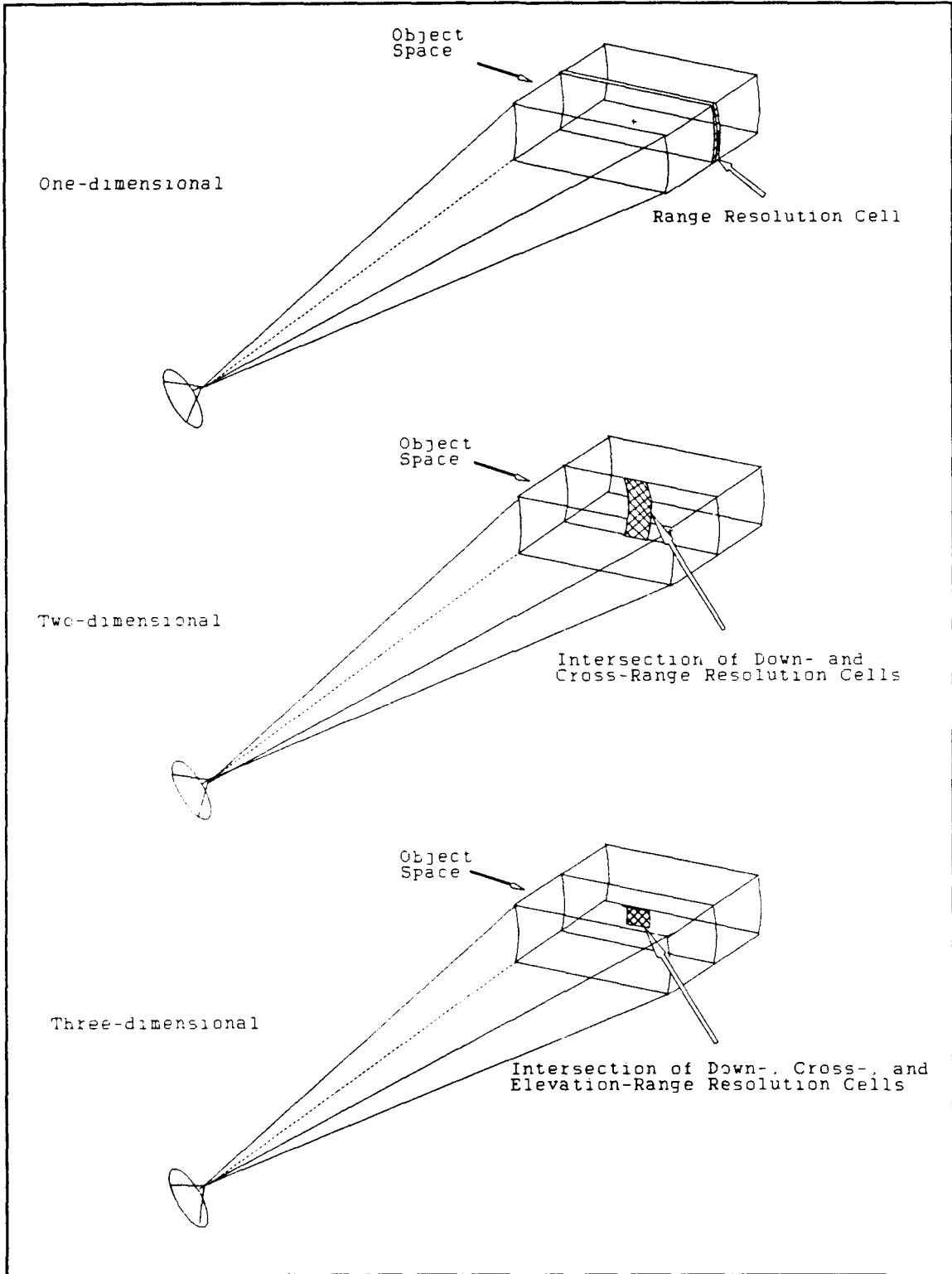
Figure 2.3 High Resolution RCS Measurements (3:373)

2-5

All three of the measurements illustrated in Figure 2.3 can be called a radar image. Therefore, most authors define a radar image as the spatial distribution of reflectivity corresponding to the discrete scattering centers on the object (3:370; 10:1). This definition is consistent with the IEEE definition which states that an image is "a spatial distribution of a physical property such as radiation, electric charge, conductivity or reflectivity, mapped from another distribution of either the same or another physical property" (7:361).

The concept that an object can be defined as a collection of discrete scattering centers, coupled with a desire to map the distribution of these scattering centers requires the ability to distinguish between closely spaced object characteristics. The following sections of this chapter will break the two-dimensional mapping process into its orthogonal components, namely range resolution and cross-range resolution.

2.2 Range Resolution

Determination of scattering center locations on the basis of range is the most fundamental imaging method. As we saw earlier this range measurement is the only method employed in making the one-dimensional measurements and is an integral part in both the two-dimensional and three-dimensional measurements as well. This section presents the theory of range resolution using a narrow pulse radar waveform. This will be followed by a presentation of two other types of radar systems

used for achieving fine range resolution. The section will close with the Nyquist sampling requirements for frequency/range measurements.

2.2.1 *Range Measurements*. The determination of the range to an object is accomplished by measuring the round trip time delay of the transmitted signal and computing the distance knowing the propagation velocity. Thus, range measurement is essentially a time delay measurement. The pulse radar waveform is conceptually the easiest waveform to visualize the relationship between pulse width and range resolution. The leading and trailing edges of the pulse radar waveform provide time markers by which the range to a scatterer may be measured. The round trip propagation delay τ for a scatterer at range R is $\tau = 2R/c$ where c is the propagation velocity (speed of light for free space). Let $\Delta\tau$ be the propagation delay difference between the leading and trailing edges of a radar pulse of duration T. The propagation delay difference between the leading and trailing edges of the pulse is $\Delta\tau = T = 2\Delta R/c$. Thus, for a radar with a pulse duration of T the range increment is given by $\Delta R = cT/2$ (3:373;10:10). Figure 2.4 shows two point scatterers separated by a distance D. As long as these scatterers are separated by a distance greater than the range increment, ΔR, the radar will receive two distinct return pulses. However, if the scatterers lie closer than ΔR, the echo returns will overlap in time and the radar will be unable to distinguish the scatterers. Therefore, to resolve closely spaced scatterers requires the transmission of narrower pulsewidths or, equivalently, increasing the bandwidth B, since $BT \approx 1$ for a rectangular envelope pulse. This relationship leads to the
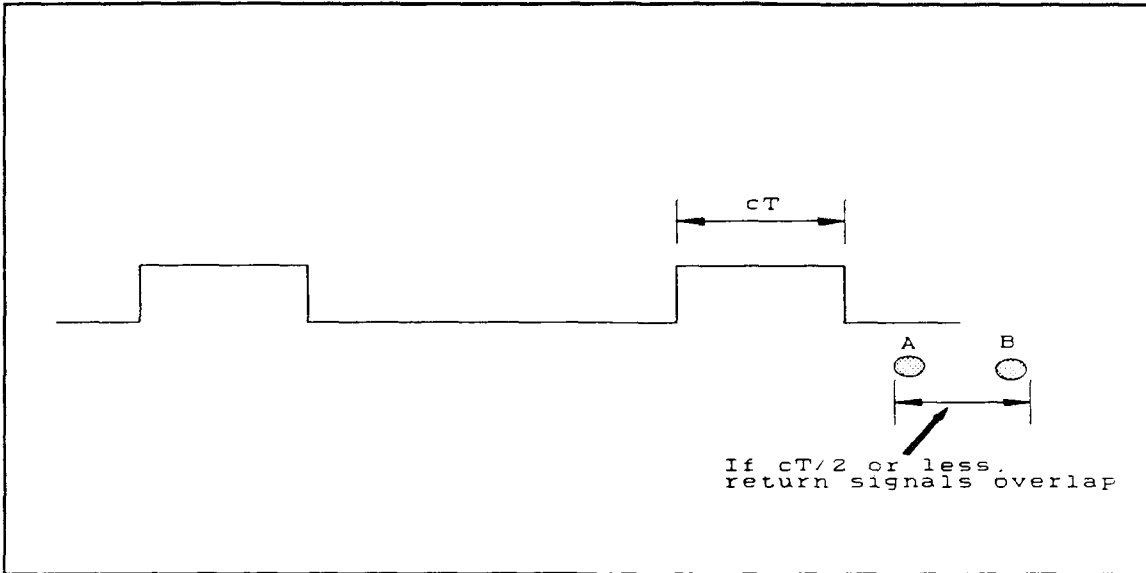
Figure 2.4 Pulse Waveform with Closely Spaced Scatterers

definition of range resolution given by

$$\Delta R = k \frac{c}{2B} \qquad (2.2)$$

where the constant of proportionality, k, is greater than one, c is the velocity of propagation and B is the radar frequency bandwidth. The exact value of k depends upon the time-bandwidth product of the particular radar waveform and on the use of weighting functions during subsequent processing (3:131,373; 10:41). Generally, when calculating the expected range resolution, k is allowed to equal one.

Figure 2.5 shows a three-dimensional object observea by a radar using time-delay sorting. Using time-delay sorting to measure the object will produce a trace of the object's scattering centers in a plot of magnitude versus distance. This trace is often referred to as a range profile. The range sorted echo from each range cell of the object will be the coherent summation of all the scattering centers contained
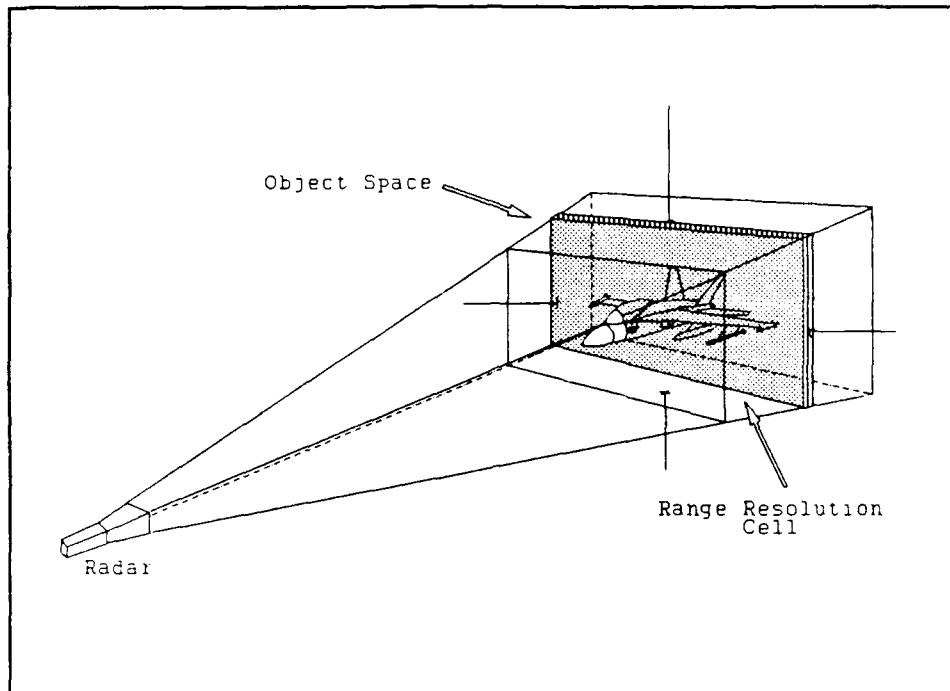
Figure 2.5   Range Profile Measurement (9:12)

in the cell, Equation 2.1 applies for each range cell.   The range

profile is therefore a cell by cell sequence of the magnitudes produced

by the coherent summation of signals from all scatterers contained in

the range resolution cells (10:11-12).

2.2.2 Comparison of Radar Waveforms.   In the previous section the

range resolution equation was developed using the pulse radar waveform.

However, as the pulsewidth of this type of system decreases the peak

power of the waveform must be increased to maintain the signal to noise

ratio.   For realistic transmitters having a fixed peak power, this type

of waveform is of limited use in imaging (3:375; 11).   Therefore, this

section discusses two other common radar waveforms and compares their

utility in radar imagery.   The radar waveform covered will be linear FM

and stepped frequency CW. Linear FM is chosen due to its overall high ratings as an imaging waveform. Stepped CW is chosen since it is the waveform used in the AFIT Anechoic radar system. The waveforms are rated using the following performance criterion: sensitivity, dynamic range, range resolution, and ambiguities.

The performance criterion are defined as follows. The optimum system sensitivity is achieved when the radar receiver is matched to the signal waveform. Thus, the matched-filter receiver establishes the upper bound of possible system sensitivity performance. The measurement criterion used for system sensitivity is the S/N (signal-to-noise) ratio. For a signal in the presence of white noise, the output of the matched-filter has a S/N ratio of

$$\frac{S}{N} = \frac{2E}{N_o}$$

where E is the signal energy and N_o is the one-sided power spectral density of the noise.

The dynamic range requirement of a system is established by the range over which the return signal may vary. Most targets of interest have rather small returns compared to the spurious returns that may arise from antenna coupling or reflections from the test range itself. If the system does not reject these signals before the receiver, the dynamic range of the receiver must be sufficient enough to handle the strong spurious signals without affecting the weaker target signal.

The range resolution requirement, given by Equation 2.2, shows that the primary requirement for achieving fine range resolution is a wide system bandwidth.

Ambiguities can arise when continuous signals are sampled for digital processing. These ambiguities take the form of aliasing errors that arise when the sampling increment increases. Taking the Fourier transform of signals containing aliasing errors will result in ambiguous responses which cannot be distinguished from the true response. Since the Fourier transform is used to find the range response of a target the system may be susceptible to aliasing errors. Therefore, systems must provide protection to avoid ambiguous range returns.

In the linear FM system, the frequency of the transmitted signal is linearly swept over a wide bandwidth and the return signal is processed in a homodyne receiver. The receiver output is a tone burst with a duration equal to the sweep period and will have a frequency proportional to the target range. For a receiver bandwidth equal to the inverse sweep duration $B=1/T$, a matched filter response is implemented for a target at a single range. Processing the receiver output through a Fourier transform is equivalent to processing the output through a bank of matched filters each set to match contiguous range cells. Thus, the sensitivity of the linear FM system will provide optimum performance. Aliased target returns may be rejected by low-pass filtering the output of the receiver. The use of range gating before the receiver will reduce the dynamic range requirements of the system

while providing protection from strong interfering echoes and antenna leakage.

The stepped CW waveform is a digital equivalent of the linear FM waveform. A stepped CW system measures the magnitude and phase of the return signal as the operating frequency is stepped in discrete increments. To achieve a matched filter response and thus the optimum signal-to-noise ratio requires that the dwell time for each frequency be the inverse of the bandwidth. Processing the phase and magnitude returns through an IFFT will yield range profiles of the target reflectivity. This system thus provides optimum performance in terms of range resolution and signal-to-noise ratio. However, the utility of this system is limited by the lack of signal rejection for signals originating outside the range of interest and the system is vulnerable to ambiguous range responses that arise from the frequency sampling process. The lack of signal rejection requires the dynamic range of the system to be large enough to accommodate strong spurious signals. The lack of anti-aliasing range filtering requires the a priori knowledge that no aliased response can occur. In chapter three these problems will be address with regard to the radar system in the AFIT anechoic chamber.

2.2.3 Nyquist Sampling Criterion for Frequency. (3:300-301) Range resolution, which is highly dependent on the total frequency bandwidth, and the number of data samples taken over this frequency bandwidth are closely related. Remembering that the bandwidth $B = f_2 - f_1 = \Delta f$, Equation 2.2 can be rewritten as

$$\Delta R = \frac{c}{2B} = \frac{c}{2(f_2 - f_1)} = \frac{\lambda}{2\Delta f/f} \qquad (2.3)$$

where the k in Equation 2.2 has been set equal to one. If the frequency band is synthesized by transmitting discrete frequency steps, the number of frequency steps required must meet or exceed the Nyquist sampling criterion of at least one sample for every 180° phase change of the transmitted signal. Therefore, the minimum frequency step size will be a function of the maximum range dimension, R_{max}, as given by

$$2\pi(\Delta f)t = 2\pi(\Delta f)\frac{R_{max}}{c} < \pi \qquad (2.4)$$

where t is the time required by the energy to travel the maximum range dimension. Solving the inequality for Δf yields

$$\Delta f = \frac{c}{2R_{max}} \approx \frac{\lambda f}{2R_{max}} \qquad (2.5)$$

Defining the number of frequency samples, $N_f = (f_2 - f_1)/\Delta f$, the Nyquist sampling criterion requires a minimum of

$$N_f = \frac{f_2 - f_1}{\Delta f} = \frac{c/2\Delta R}{c/2R_{max}} = \frac{R_{max}}{\Delta R} \qquad (2.6)$$

frequency samples. In practice, the frequency band is over sampled to ensure that the complex structure of the return is preserved in the measurement. Also, since the data is often processed using an FFT, it is convenient to collect at least the next higher power of two number of samples than is required by the Nyquist criterion.

2.3 Cross-Range Resolution

In this section the second dimension required for two-dimensional imaging, cross-range resolution, is presented. The most common type of processing used in obtaining the cross-range dimension is Doppler processing. Thus the theory will be initially developed along this "classic" line. This will be closely followed by an equivalent method using stationary observations. This section will close with a look at the Nyquist sampling criterion for the cross-range direction.

2.3.1 Cross-Range Measurements. (21:277-279; 3:386-388) The basis of Doppler processing is that an object moving relative to a stationary radar will have a radial component of velocity which causes a shift in the frequency of the returned signal. This frequency shift is directly proportional to the radial component of velocity of the object relative to the radar (10:12). Figure 2.6 depicts the special case employed by ISAR of an object rotating about a central axis and a stationary radar. Assuming the distance between the radar and an object is large, the Doppler frequency shift of a scatterer located at a cross-range distance x on an object rotating with a constant velocity ω will have an instantaneous velocity ωx toward the radar, as depicted. The Doppler frequency shift produced by the object rotated through a small angle is given by:

$$f_D = 2\omega x \frac{f_c}{c} \tag{2.7}$$

where f_c is the center frequency or the carrier frequency of the radar and c is the propagation velocity. Let us now consider two scatterers
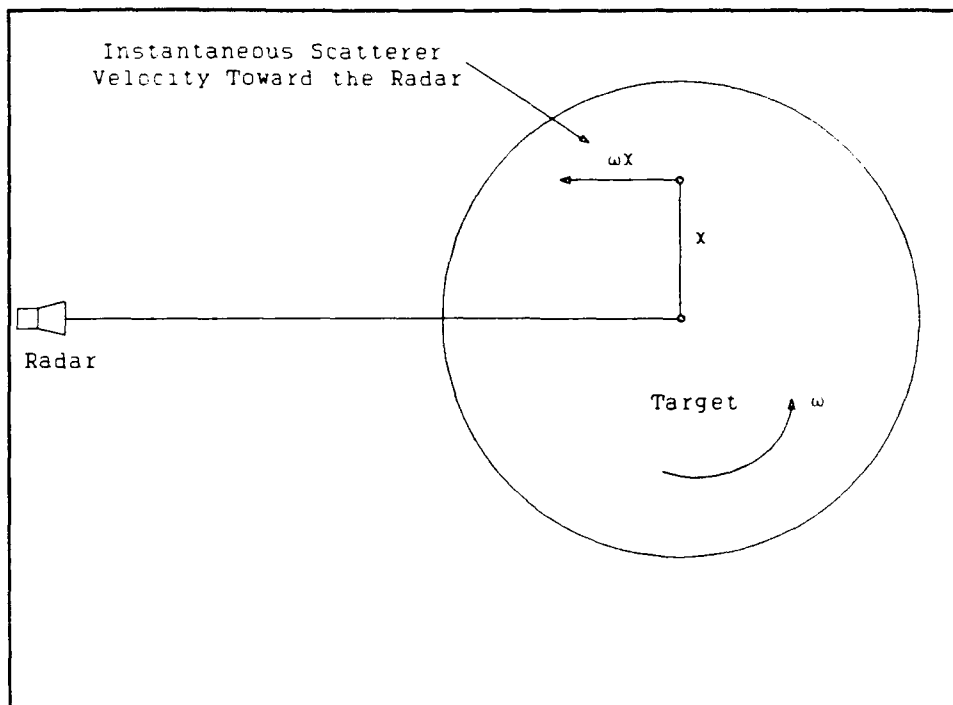
Figure 2.6 Radial Velocity Produced by a Scatterer on a
Rotating Object (19:277; 3:386)

in the same range cell separated by a cross-range distance Δx as shown
in Figure 2.7. The velocities of the point scatterers will be $V_1 = \omega x_1$
and $V_2 = \omega x_2$ .The difference in these velocities is given by $\omega \Delta x = V_2 - V_1$
and the corresponding frequency difference is

$$\Delta f_D = 2\omega\, \Delta x\, \frac{f_c}{c} \qquad (2.8)$$

If Δf_D is the Doppler frequency resolution of the radar, then
rearranging Equation 2.8 yields the cross-range resolution
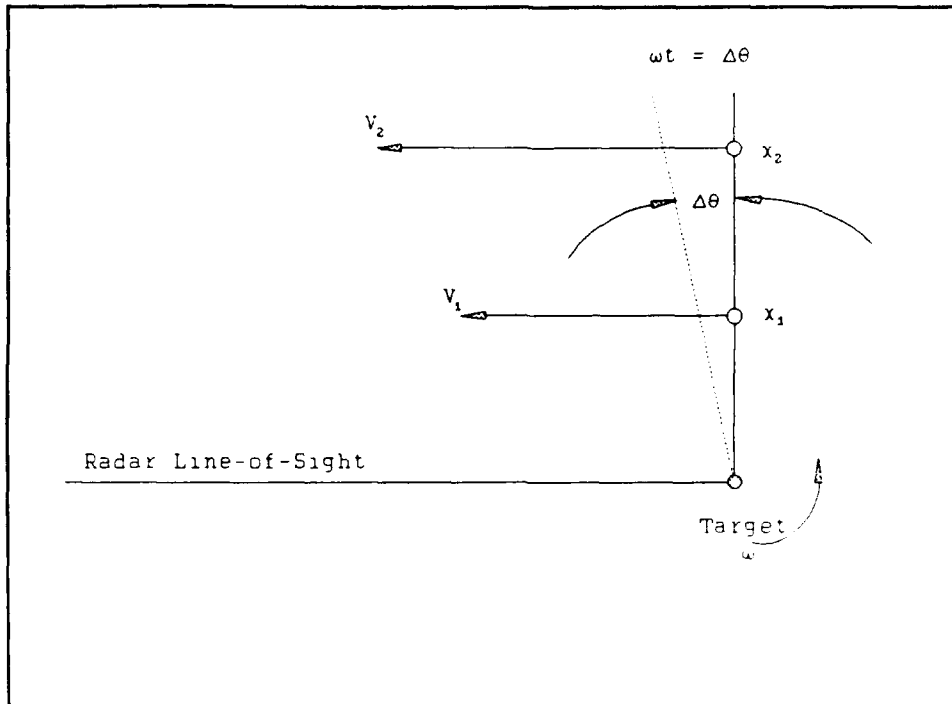
Figure 2.7 Cross-Range Resolution Geometry - Two Scatterer
Case (3:88)

$$\Delta x = \frac{c \, \Delta f_D}{2 \omega f_c} \tag{2.9}$$

However, the Doppler resolution can be related to the coherent
integration time t by the approximation

$$\Delta f_D \approx \frac{1}{t} \tag{2.10}$$

Thus, the cross-range resolution may be expressed as

$$\Delta x = \frac{c}{2 \omega t f_c} = \frac{\lambda}{2 \omega t} = \frac{\lambda}{2 \Delta \theta} \tag{2.11}$$

where λ is the wavelength of the center or carrier frequency and $\Delta \theta$ is
the total angle viewed during the integration time t. The relationship

2-16

in Equation 2.11 holds true as long as the angle $\Delta\theta$,expressed in radians, is small.

Thus the cross-range resolution is proportional to the wavelength and inversely proportional to the observation angle viewed during the integration time. There is a temptation to achieve some desired cross-range resolution by increasing the observation angle. Unfortunately, allowing $\Delta\theta$ to increase beyond the small angle approximation will cause the scatterers to migrate from the range cell of origin to adjacent range cells during the integration time. This migration causes blurring of the scatterers in the image. There is, however, a solution to this problem, called focusing. The subject of migration through range cells and the focusing of images will be covered in the next section of this chapter.

Mensa (10:12-15) develops the cross-range processing in a slightly different manner which emphasizes the equivalence between temporal Doppler processing and angular Doppler processing. The equivalence between these types of Doppler processing allows the AFIT anechoic chamber radar system to be used for two-dimensional image data collection. Therefore, Mensa's development of cross-range resolution will also be reviewed with specific attention paid to the equivalence of the two types of processing.

Figure 2.8 depicts the geometry used by Mensa in which a scatterer is located a distance d from the center of rotation of an object rotating with an angular velocity ω. At any given time t the distance r to a distant ($R_o \gg d$) antenna is
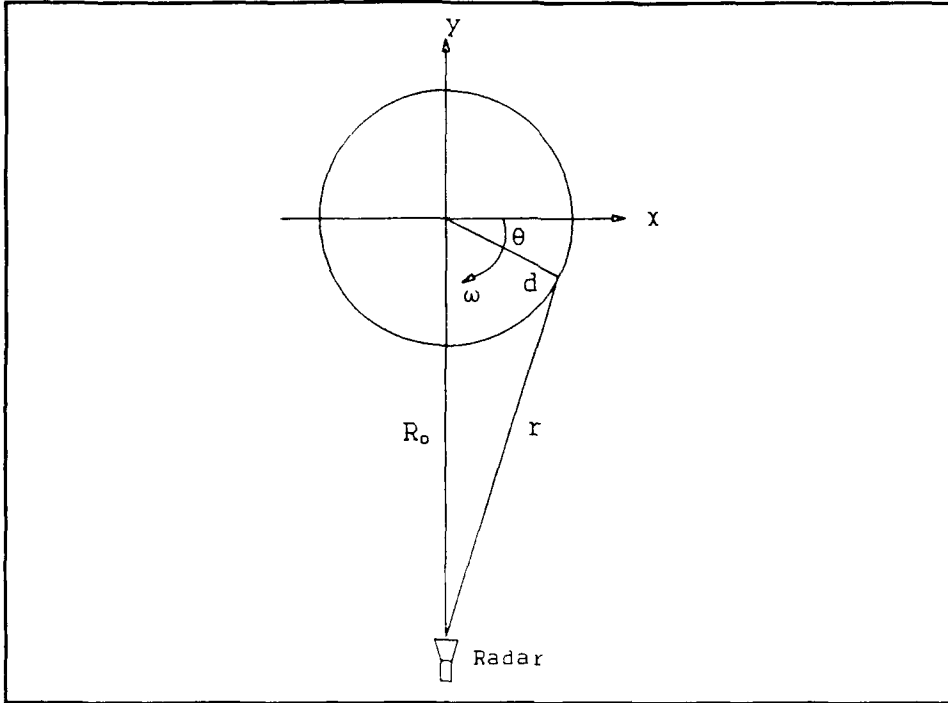
Figure 2.8   Rotating Object Geometry (9:14)

$$r = R_o - d\sin(\omega t) = R_o - d\sin\theta \qquad (2.12)$$

where θ is the rotation angle, measured clock wise from the x axis, as shown. If the object's motion is negligible during the signal round trip travel time the received signal ($e_R(t)$) is a replica of the transmitted signal ($e_T(t) = Re[\exp(j2\pi ft)]$) delayed by the round trip time $2r/c$, which is given by:

$$e_R(t) = Re\{\exp[j2\pi ft - j4\pi R_o/\lambda + j(2\pi/\lambda)2d\sin(\omega t)]\} \qquad (2.13)$$

The first term in the argument of the exponential is the carrier phase; the second term is the phase shift due to the round-trip delay associated with the range R_o. The third term is the Doppler shift due

2-18

to the varying range. This Doppler shift can be expressed as a function of either time or the rotation angle, but in either case the effect described is the change in the phase of the received signal due to changes in the round-trip distance.

The Doppler frequency may be expressed as the temporal phase rate of change of the envelope of the complex return signal

$$f_t = \frac{1}{2\pi} \frac{d\phi}{dt} = -\frac{2}{\lambda} \frac{dr}{dt} = 2\omega \frac{d}{\lambda} \cos(\omega t) = \frac{2\omega x}{\lambda} \qquad (2.14)$$

where f_t is the temporal Doppler frequency, ϕ is the total phase shift in the received signal represented by the last two terms of the exponent of Equation 2.13, and x is the cross-range distance. The Doppler frequency may also be expressed as the angular phase rate of change by

$$f_\theta = \frac{1}{2\pi} \frac{d\phi}{d\theta} = -\frac{2}{\lambda} \frac{dr}{d\theta} = 2 \frac{d}{\lambda} \cos(\theta) = \frac{2x}{\lambda} \qquad (2.15)$$

Where f_θ is the angular Doppler frequency and the rotation angle θ is given by $\theta = \omega t$. Notice that Equations 2.14 and 2.15 are proportional to the instantaneous cross-range distance and differ by only the scale factor ω.

When temporal Doppler processing is used, the object is rotated at a constant angular rate and the complex envelope of the returned signal is recorded. With angular Doppler processing the object is stepped in uniform angular increments with a static measurement of the relative phase made at each angle. Due to the equivalence of Equations 2.14 and 2.15 the processed signals recorded as a function of angle will yield

2-19

identical results as signals recorded as a function of time for a fixed rotation rate ω.

The direct relationship between the Doppler frequency and cross-range distance allows spectral analysis of the signal to separate the contributions of many reflecting points on the basis of cross-range position. The resolution of the Doppler frequency f_t varies inversely with the processing time t, $\Delta f_t \approx 1/t$. Therefore, the cross-range resolution is once again given by:

$$\Delta x = \frac{\lambda}{2\omega} \Delta f_t = \frac{\lambda}{2\omega} \frac{1}{t} = \frac{\lambda}{2\Delta\theta} \qquad (2.16)$$

where $\Delta\theta$ is the angular rotation during the processing time t. Again, this equation is true for small angles $\Delta\theta$.

By performing a Fourier transform, the multiple Doppler frequencies present in the signal can be separated. Figure 2.9 depicts a three-dimensional object being imaged by Doppler processing; resolution is along an axis normal to the axis of rotation and to the radar line-of-sight. Unlike the range profiles mentioned earlier which can be associated with specific aspect angles, the cross-range profiles require that the object rotate through a range of angles due to the Doppler processing used to obtain the cross-range resolution.

2.3.2 Nyquist Sampling Criterion for Angle. (3:301-302) The cross-range resolution depends on the total angle $\Delta\theta$ over which the data is collected and was given by
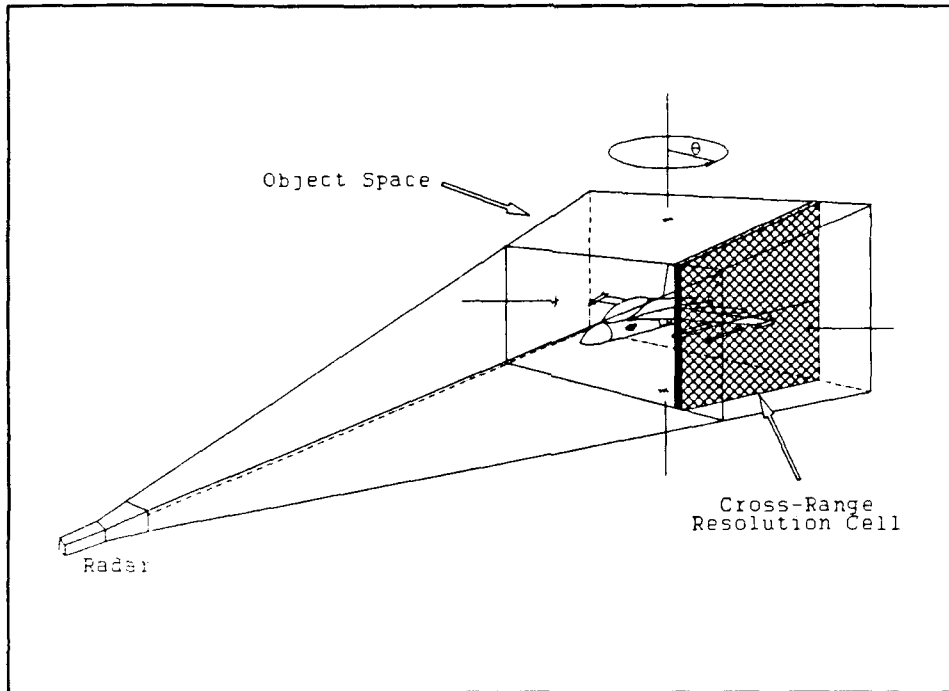
Figure 2.9 Cross-Range Measurement (9:19)

$$\Delta x = \frac{\lambda}{4\sin(\Delta\theta/2)} \approx \frac{\lambda}{2\Delta\theta} \qquad (2.17)$$

where λ is the center wavelength (10:56). The Nyquist criterion states that the maximum phase change can be no more than 180° in the cross-range direction.   Thus, if the angle between the frequency observations is defined as $\delta\theta$ the minimum angular step size will be a function of the maximum cross-range dimension, x_{max}, as follows

$$4\pi\frac{x_{max}}{\lambda}\delta\theta < \pi \qquad (2.18)$$

Solving this equation for $\delta\theta$ yields

$$\delta\theta < \frac{\lambda}{4x_{max}} \qquad (2.19)$$

Defining the number of angle samples as $N_\theta = \Delta\theta/\delta\theta$, and using Equations 2.17 and 2.19 the minimum number of angle samples required by the Nyquist sampling criteri n is

$$N_\theta = \frac{\Delta\theta}{\delta\theta} = \frac{\lambda/2\Delta x}{\lambda/4x_{max}} = \frac{2x_{max}}{\Delta x} \qquad (2.20)$$

As in the case of frequency sampling the number of angle samples is often much greater than the Nyquist criterion and is generally allowed to be at least the power of two higher than Equation 2.20 requires.

2.4 Focused and Unfocused Images

As mentioned briefly earlier, a radar image will be blurred by the migration of scattering centers through resolution cell if the data is collected over too large of an angular aperture. This section develops the subject of the motion of scattering centers through resolution cells presenting the limitations that this motion imposes on the collection process, the solution to this problem, and finally a discussion of the relative merits of small angular aperture images versus large angular aperture images.

2.4.1 Motion of Scattering Centers through Resolution Cells. As mentioned earlier, the processing of the radar return versus frequency and angle data is carried out by applying a Fourier transform to the frequency response at each of the $\delta\theta$ collection angles to obtain the

2-22

range resolution, and applying a subsequent set of Fourier transforms to each range cell to obtain the cross-range resolution. For any given frequency response (i.e., fixed aspect angle), the Fourier transform is the exact computation needed to obtain the range resolution. However, as the object rotates, the range to a given scatterer will change causing a migration in the apparent range location. Because of this migration the Fourier transform becomes only an approximation to the exact computation needed for obtaining range and cross-range resolutions. The rotation of the target has induced a coupling between the range and cross-range resolutions that the approximation ignores. Thus, the migration of a scattering center through the resolution cells will result in blurred images. To achieve a given resolution it is necessary for the motion of a scatterer to be limited to its initial resolution cell (12:1). Since the motion of a scatterer will be most extreme at points furthest from the center of rotation, two cases examining these extremes will the investigated.

Figure 2.10a shows a scatterer located at the edge of an object, 90° to the radar line-of-sight. Rotational motion will cause this scatterer to migrate from one range cell to an adjacent range cell. If the width of the object in the cross-range direction is D_x, then the scatterer will move $1/2\ D_x\Delta\theta$,for small values of $\Delta\theta$. To restrict the motion of the scatterer to a single range resolution cell, the following inequality must apply
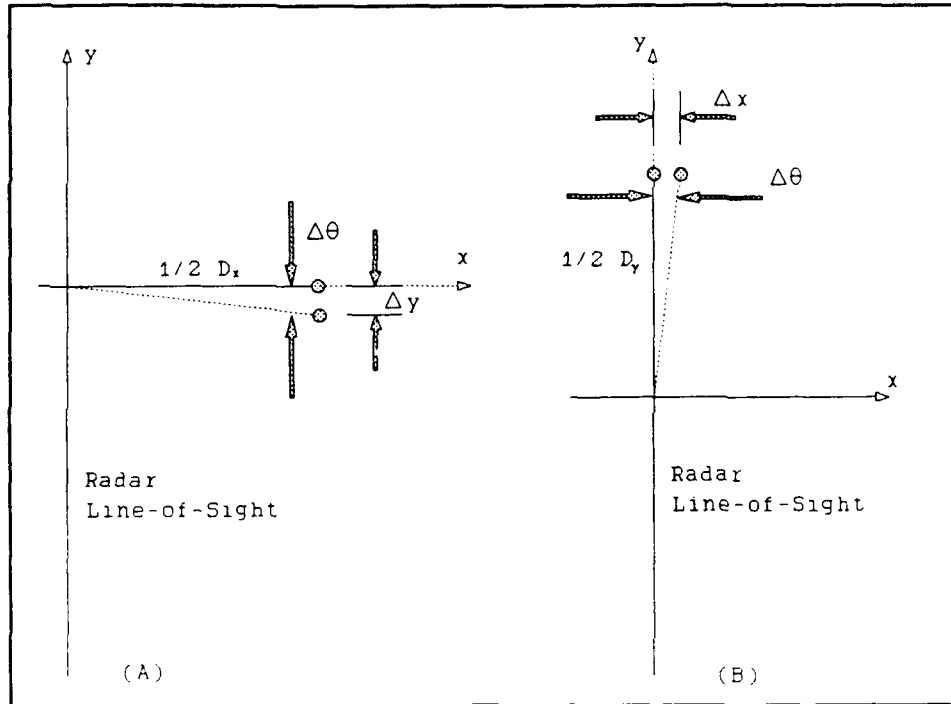
Figure 2.10 Geometry of Scatterer Migration through
Resolution Cells

$$\frac{1}{2}D_x \, \Delta\theta \le \Delta R = \Delta y \qquad\qquad (2.21)$$

Solving Equation 2.11 for $\Delta\theta$ and substituting the result into Equation
2.21 yields the following limitation on the range resolution

$$\Delta y \ge \frac{\lambda D_x}{4\Delta x} \qquad\qquad (2.22)$$

The case shown in Figure 2.10b provides the limitation on the cross-
range resolution. To prevent a scatterer located at the edge of an
object and in line with the radar line-of-sight from migrating beyond
its initial resolution cell, the following inequality must hold

$$\Delta x \geq \frac{1}{2} D_y \Delta \theta \qquad\qquad (2.23)$$

where Δx is the cross-range resolution, D_y is the width of the object in the range direction. Once again, substituting for $\Delta \theta$ yields the limitation on the cross-range resolution

$$(\Delta x)^2 \geq \frac{1}{4} \lambda D_y \qquad\qquad (2.24)$$

Equations 2.22 and 2.24 are the relationships that Brown and Walker (2:98; 20:23) use in specifying the limitations imposed on the range and cross-range cell sizes by the migration of scatterers through resolution cells. Mensa (12:1) has combined these expressions in his paper by making the following simplifications: the range and cross-range object widths are set equal to one another, $D_x = D_y = L$; the range and cross-range resolutions are set equal to one another, $\Delta x = \Delta y$. Using these simplifications, Equations 2.22 and 2.24 each yield the following equation

$$(\Delta x)^2 \geq \frac{1}{4} \lambda L \qquad\qquad (2.25)$$

where Δx is either the range or cross-range resolution and L is the maximum target extent. Now, squaring Equation 2.11 and substituting into Equation 2.25 yields Mensa's relationship between the maximum target extent and the total angular aperture over which the target is viewed

$$\frac{\lambda}{\Delta\theta^2} \geq L \qquad\qquad (2.26)$$

Mensa goes on to define the extent of image blurring based on Equation 2.26. A scatterer located at the center of rotation does not move in either the range or cross-range direction as the object rotates, thus such a scatterer is imaged at the maximum achievable resolution of $\lambda/2\Delta\theta$. As the location of the scatterer moves out from the center of rotation the blurring increases. For a scatterer located at distances less than $\lambda/2\Delta\theta^2$ the amount of image blurring will be minor. If a scatterer is located beyond L/2, where L is the distance given by Equation 2.26, the blurring approaches $r\Delta\theta$, which is the length of the arc traveled by a scatterer located a distance r from the center of rotation. Figure 2.11 shows the relationship between the location of a scatterer and the effective resolution caused by the blurring due to motion of the scatterer.

2.4.2 Image Focusing. For data collected under the limitations of Equations 2.22 and 2.24, or equivalently Equation 2.26, the Fourier transform is nearly the exact solution for determining the range and cross-range coordinates of the scattering centers. However, these equations place somewhat severe restrictions on the cross-range resolution (and the range resolution if the two are held equal) due to the limitations on the total angular aperture, $\Delta\theta$. There is a way of overcoming the limitations imposed by Equations 2.22, 2.24, and 2.26. To understand the limitations requires a look at how the data is disposed on the collection grid and how the Fourier transform requires
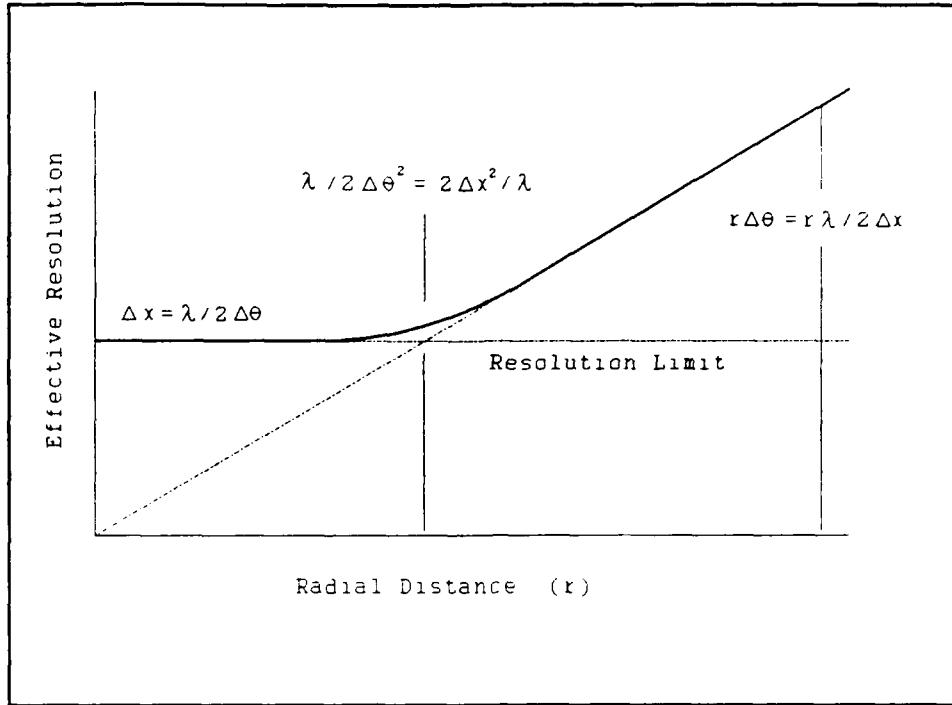
Figure 2.11   Resolution Degradation due to Target Motion
(11:4)

the data to be disposed.   Figure 2.12 shows both the data collection

grid and the grid required by the Fourier transform.   The closed circles

are the collected data points, which lay along radial lines spaced at

equal frequency increments.   The open circles represent the placement of

the data points required by the Fourier transform; these points are

spaced equally in the range and cross-range direction.   Notice, for

small angular apertures the two grids nearly coincide.   This coincidence

allows the direct application of the Fourier transform on the data

collection grip for small angular apertures.   For large angular

apertures the grids differ greatly and direct application of the Fourier

transform will result in blurred images.   To correct the problem
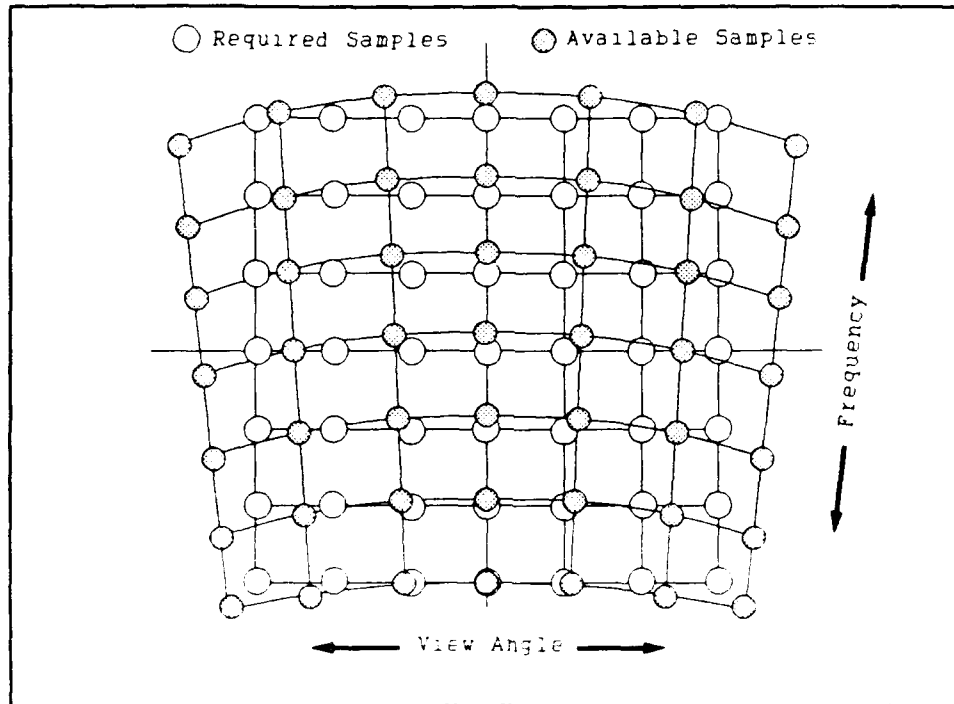
Figure 2.12   Polar Formatted Data Versus Rectangular
Formatted Data (8:23)

requires the reformatting of the frequency/angle coordinates from a

polar format to a rectangular format.   Figures 2.13 and 2.14 pictorially

present the polar reformatting process.   The first step in the polar

reformatting process, shown in Figure 2.13, is to interpolate the

frequency data along the constant azimuth lines to form straight range

lines, sometimes known as a "keystone raster" (9:60; 21:316; 12:3).

The second step in focusing the image is to interpolate the data from

the keystone grid to the final rectangular grid, shown Figure 2.14.

(It should be noted here that for systems in which the target continues

to rotate during the data collection time, as opposed to the method used

in this thesis, the collected data samples will have a skewed fan-shaped
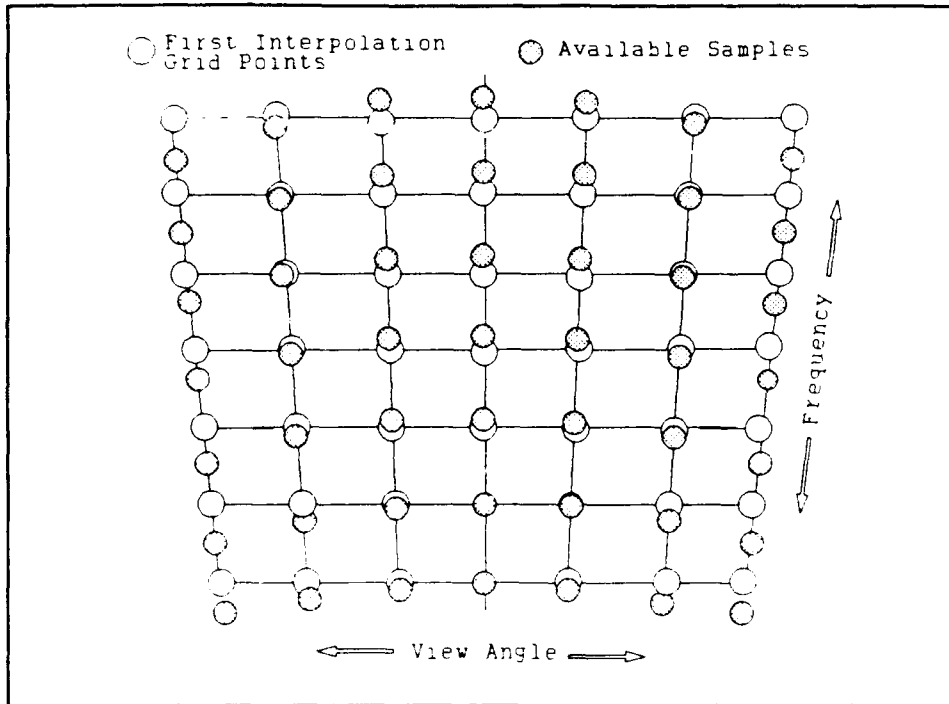
Figure 2.13 Polar to Rectangular Interpolation   Step One
(19:316)

distribution (3:397; 21:315). Before applying the two steps described

above, the skewed data must be interpolated to a polar grid.) Mather

(9:2   indicates that to achieve the maximum resolution it is important

to interpolate from the polar grid to the largest rectangular grid which

will inscribe the annular section.

The elegance of this technique for image focusing is that the data

array is corrected once for the entire target space. The even spacing

of the rectangular grid allows the application of the computationally

efficient FFT algorithms and will result in focused images regardless of

the size of the angular aperture over which the data was collected.

Thus it is possible to ignore the small angle restriction mentioned

2-29
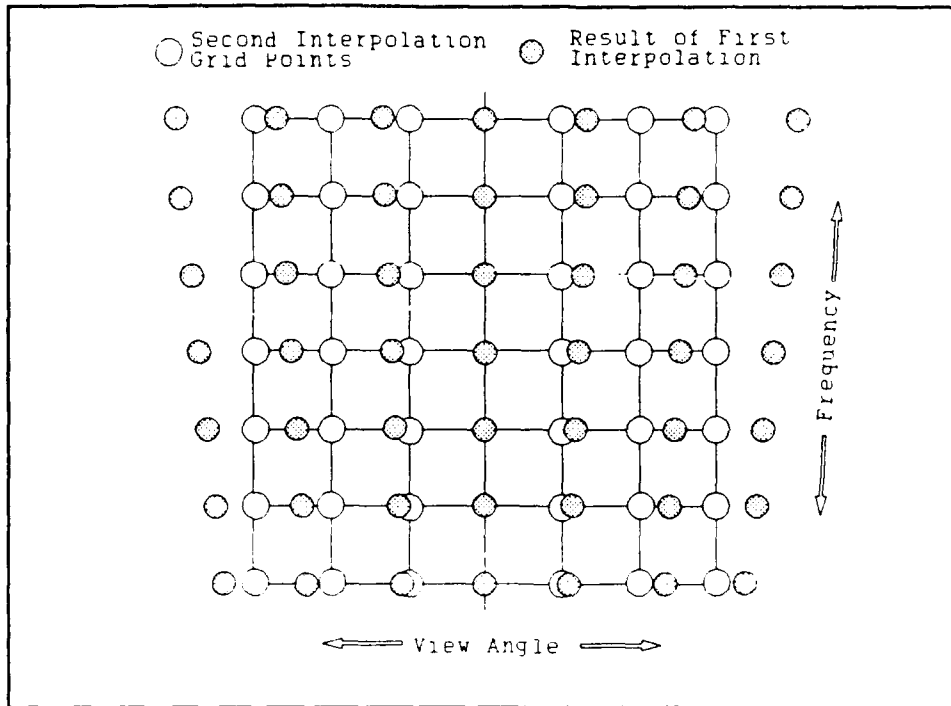
Figure 2.14   Polar to Rectangular Interpolation Step Two
(19:316)

earlier and collect data over large apertures to achieve a given cross-range resolution.   The question that arises from such a measurement is: "What exactly does the image represent?"   This question will be addressed in the next section of this chapter.

   2.4.3   RCS versus other Images.   The radar imaging authorities are split on their interpretation of how large of an angular aperture should be allowed when generating an RCS image.   Walker in his work at the Environmental Research Institute of Michigan has observed an improvement in both the range and cross-range resolution of focused images with increased angular aperture $\Delta\theta$ and provides several images collected over increasing angular apertures of up to 90° as proof (20:37-39).   Mensa

(12:2-3) also seems to advocate the use of large angular apertures, at least to the point that some desired cross-range resolution is achieved, for obtaining high resolution images. The authors for Currie's book, however, advocate the use of small angular apertures. Horst and Shaeffer state that "... the microwave image requires a narrow field of view." (3:296) and even go on to cite Walker's resolution limitation equations (3:302) without mentioning the remainder of Walker's work in image focusing. Kurtz and Scheer write:

> "In order for the ISAR assumptions to hold, the target dimensions are required to be small relative to the radar beam, and also required is that the images are obtained from observations over small segments of viewing angle." (3:387)

These gentlemen also cite Walker's work in regard to image focusing, but only focus their data array to correct for the skewing of the data due to target motion during the observation time (3:396-397). They do include a composite image of a Volkswagen Cabriolet which is made by combining images taken at 35°,40°,45°,and 50° relative to the front of the vehicle (3:424,429) which appears as if it were produced from an image collected over a large viewing angle. From the spacing of the image orientation angles one assumes that the viewing angle used was not more than 10°.

The problem here is not that we cannot focus images collected over large angular apertures, Walker has demonstrated that this can be done, but rather what is the meaning of a radar image that has been collected over an angular aperture of 30°, 40° or 90°. An image collected over large apertures is akin to visually observing the object at say nose-on and broadside at the same time. Thus, an image collected over a large

angular aperture while informative for target identification is of little practical use RCS measurements since it is really a composite view of the target and a radar viewing the target from a single angle would not observe the characteristics displayed in such a composite.

Radar images are used in two very general categories, target identification and RCS reduction diagnostics. For target identification, the general consensus for images appears to be that the angular aperture should be held as large as possible so that high quality "pictures" of the object or terrain can be obtained. In the area of RCS reduction diagnostics, where the aim is the identification of "hot spots" that require additional attention in an effort to reduce the target's total RCS signature, large angular apertures are sometimes used in an effort to increase the cross-range resolution. Although this provides a high resolution image, it can no longer be called an RCS image. Assume that one is interested in the RCS of an aircraft in a conical region of 20° half-angle centered on the nose of the aircraft, as depicted in Figure 2.15. Assume that the RCS is very low for any radar direction within this cone, but that a large RCS occurs 10° or 20° outside the cone. Assume further that one attempts to create a "high resolution RCS image" for the nose-on direction by using a large angular aperture centered on the nose. The large RCS will be observed within the large angular aperture, but outside our conical region of interest. The source of this large RCS will be imaged to its proper location on the aircraft, but the resulting hot spot on the image does not apply to our nose-on region of interest. In short, we have a high
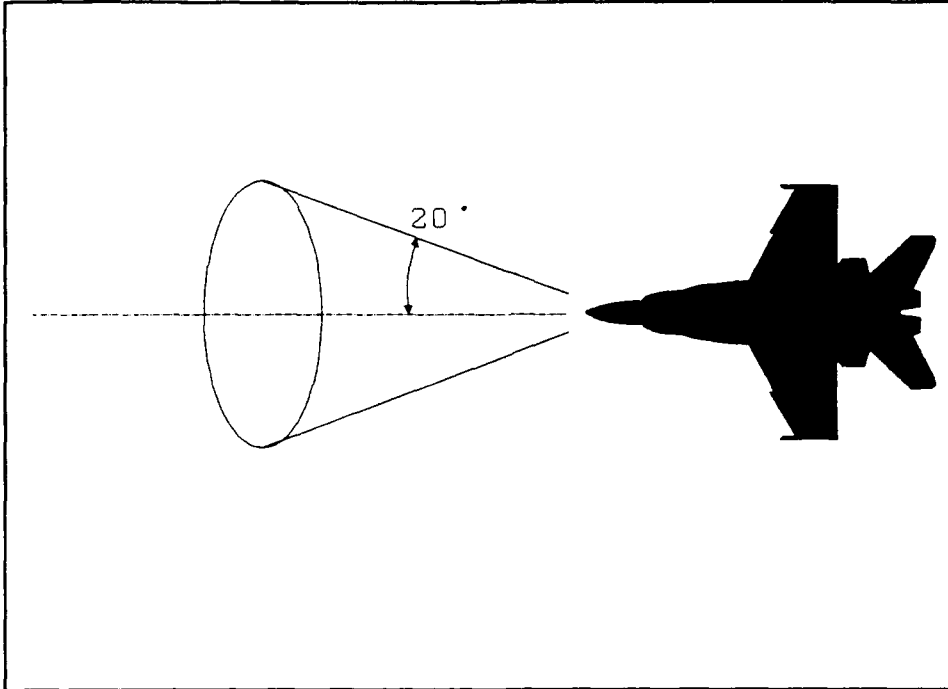
Figure 2.15   Aircraft Signature Region of Interest.

picture of the wrong thing.   Furthermore, one must realize that in any

two-dimensional radar image the data has been averaged in two

dimensions.   The magnitude of any point in the image represents the

average RCS of that point for the frequency range and angular range over

which it was measured.   In the end, it is in the interest of the person

analyzing the image to be aware of what he or she is really looking at.

2.5 Data Processing

In this section the data processing required to form an image is

discussed.   As mentioned often prior to this point, the Fourier

transform and primarily the Discrete Fourier Transform (DFT) or Fast

Fourier Transform (FFT) are used to obtain the complex reflectivity map

of the scattering centers. Thus, the rationale for the use of the Fourier transform will be presented. Other subjects that apply to data processing are: the use of weighting functions, or windows, to minimize or eliminate the processing sidelobes; and image focusing, a topic that was developed to some degree in the last section.

2.5.1 Fourier Transform Processing. In Section 2.2 the range resolution of a target was derived from a radar pulse view point and the reader was told that a Fourier transform may be used to obtain the time response, and hence the range response, from the complex frequency response of an object. In this section the theory is presented in a more general form which will introduce the use of Fourier transforms to radar image processing.

To distinguish closely spaced scatterers requires resolving *signals* having small differences in time delay. To achieve this requires the use of a signal waveform which is as different from its shifted self as possible. This requirement leads one to the autocorrelation function which is expressed as

$$R(\tau) = \int_{-\infty}^{\infty} S(t) \, S^*(t+\tau) \, dt \qquad (2.27)$$

where S(t) is the signal, S^*(t+τ) is the conjugate signal which has been time delayed by τ. The autocorrelation function is a real, even function which reaches a maximum at $\tau{=}0$. To distinguish between nearly equal time delays requires that the autocorrelation function fall sharply with increasing τ; thus, the ideal response for the autocorrelation function is an impulse response. The autocorrelation

2-34

function and the signal power spectrum S(f) are a Fourier transform pair given by

$$S(f) = \int_{-\infty}^{\infty} R(\tau) \exp(-j2\pi f \tau) \, d\tau \qquad (2.28)$$

By invoking the uncertainty relation between Fourier transform pairs, Bt~1, one can conclude that an autocorrelation function having a narrow width corresponds to a wide signal bandwidth B. Thus to achieve a fine range resolution requires a wide bandwidth signal and the range resolution is generally given by Equation 2.2

$$\Delta R = k \frac{c}{2B} \qquad (2.2)$$

where the constant k is allowed to equal one (10:10-11; 11).

Therefore, range (or time) response may be obtained by taking the Fourier transform of the coherent frequency response, A(f), returned by the object

$$A(t) = \int_{f_1}^{f_2} A(f) \exp(j2\pi f t) \, df \qquad (2.29)$$

(3:297).

Similarly, the cross-range resolution is obtained by Fourier transforming the coherent angle data $A(\theta)$ to obtain the cross-range location of a scatterer

$$A\left(\frac{2x}{\lambda}\right) = \int_{\theta_1}^{\theta_2} A(\theta) \exp\left[j2\pi\left(\frac{2x}{\lambda}\right)\theta\right] d\theta \qquad (2.30)$$

where the cross-range x is given in units of $\lambda/2$. The angle return $A(\theta)$ is collected and stored for every $\delta\theta$ sample point and after collection of the full angular aperture, $\Delta\theta$, the angular Fourier transform is performed (3:298).

Thus the image, which will be the spatial location of the scattering centers, is obtained by taking the inverse Fourier transform of the frequency responses at each of the fixed observation angles $\delta\theta$ to obtain the range response and taking the inverse Fourier transform of the angular responses along each of the incremental frequency steps to obtain the cross-range response.

Since the frequency bandwidth is sampled to obtain the digitized response and the angular data is collected at discrete angular location the integral form of the Fourier transform (which requires continuous time and frequency) does not apply. The forms of the Fourier transform that do apply are: the Discrete Fourier transform (DFT)

$$X(\omega) = \sum_{n=1}^{N} x(n) \exp(-j\omega n) \qquad (2.31)$$

where ω is continuous and n is discrete, $X(\omega)$ is periodic in 2π for K values of ω; and the Fast Fourier transform (FFT)

$$X(k) = \sum_{n=1}^{N} x(n) \exp(-j2\pi kn/N) \qquad (2.32)$$

where k and n are both discrete and k=1 to N where N=2^P, p=integer. The primary differences between the two forms is that the FFT requires a

2-36

power of two data set while the DFT does not. This requirement on the part of the FFT is more than made up for in its speed. The FFT makes $\log_2(N)$ computations, while the DFT requires NK computations. Thus, the FFT is often the transform of choice in imaging applications where the data arrays are often limited by the size of available computer memory (11).

    2.5.2 Data Windowing. (9:75-76) The application of either the DFT or FFT on a finite data set leads to errors introduced by the strict truncation (uniform windowing) of the data. These errors are manifested as sidelobes, sometimes known as processing sidelobes, which can obscure weak return signals. These sidelobes may be reduced by the application of a weighting function or window which taper smoothly to zero near the ends of the data set. Harris (6) has catalogued many of the windows available for this use, having evaluated them on the basis of highest sidelobe level, sidelobe fall off, coherent gain, equivalent noise bandwidth, 3 dB bandwidth, and several other parameters. For imaging applications, many authors use the Hamming window for reducing the processing sidelobes. The Hamming window has the mathematical expression (6:62)

$$w(n) = 0.54 - 0.46\cos(\tfrac{2\pi}{N}n),$$
$$n = 0, 1, 2, \cdots, N-1 \qquad\qquad (2-33)$$

The reduction of processing sidelobes comes at the cost of increasing the width of the central spike. This translates into a loss of range and cross-range resolution; for the Hamming window the resolution cell size increases by a factor of 1.47 (3:385).

2.5.3 Image Focusirg. The subject of image focusing was covered in the last section in regards to the migration of scattering centers through resolution cells, thus it will not be fully repeated here. However, the main points from that discussion will be presented.

As long as the total angular aperture $\Delta\theta$ remains within the small angle approximations, the data collection grid will very nearly approximate the rectangular grid required by the Fourier transforms and the grid would not need to be reformatted. However, as the angular aperture increases beyond the small angle approximation, the data collection grid increasingly takes the shape of a section of an annulus. Thus, the data collection grid points and the data processing grid points no longer coincide. Applying a DFT or FFT directly to such a data collection grid will result in an image that exhibits blurring of the scattering centers due to the motion of the scatterers through the resolution cells. To correct blurring requires that the data collection array be interpolated to the data processing array shape.

Due to time constraints, the image focusing algorithms were left out of the data processing software for this thesis. The images that may be produced with the processing software provided are limited in the size of the angular aperture that may be collected. This limitation is most easily found by solving Equation 2.26 for $\Delta\theta$

$$\Delta\theta \leq (\lambda/L)^{1/2} \tag{2.34}$$

where L is the longest target horizontal dimension and λ is the center wavelength.

2.6 Summary

This chapter has covered the concept of objects being a collection of discrete scattering centers, the development of the range and cross-range resolution equations, the Nyquist sampling criterion for the frequency and angle directions, the related subjects of the motion of scattering centers through resolution cells and image focusing, the connection between range and cross-range resolution and the Fourier transform, and finally the subject of windowing the data array to minimize the processing sidelobes.

The equations presented in this chapter that are of primary importance in image data collection and processing are: Equations 2.2 and 2.11, which give the resolution in the range and cross-range directions; Equations 2.6 and 2.20, the Nyquist sampling criterion for the frequency and angle directions; Equations 2.22 and 2.24 or equivalently Equation 2.26, the limitations imposed by the motion of scattering centers through resolution cells, a limitation that must be enforced with this thesis since image focusing is not implemented in the data processing.

Summarizing the processing sequence that is implemented by this thesis will help to draw together the material presented in this chapter. An object is illuminated by a stepped CW waveform at incremental angular steps $\delta\theta$ over the entire angular aperture $\Delta\theta$. Each of these frequency measurements is the Fourier transform of the range profile of the object at the given $\delta\theta$ and are one column in the data array. Moving row-wise across the array is the Fourier transform of the

cross-range profile at that particular range. The complex reflectivity map of the object is created by first applying a window to the array to reduce the processing sidelobes. This is followed by the application of a two-dimensional IFFT to all the rows of the array. The magnitude of each of the complex values in the array will be found, the logarithm of each magnitude is taken, and the results are multiplied by twenty to obtain a dB magnitude reflectivity map of the object's scattering centers.

III. AFIT Chamber and Radar System

In this chapter the physical layout and radar hardware of the AFIT anechoic chamber is described. The radar system is evaluated for its usefulness in imaging applications, and those portions of the system software that were used as a basis for the imaging software are discussed. The material of this chapter is based largely on (14), where major portions of the radar processing software were developed.

3.1 Physical Layout (14:8-14)

The AFIT anechoic chamber is part of AFIT's Advanced Technology Laboratories and is located in Building 168 on Area B at Wright-Patterson AFB. The anechoic chamber is physically contained within the structure of Building 168, thus restricting the dimensions of the chamber. Figure 3.1 show the plan view of the chamber and locates the major features.

The chamber was designed several years ago when it was believed that tapered chamber walls would help to prevent the specular reflections off the walls and ceiling from reaching the receive antenna. This concept has since been disproven by Joseph (8) and Swarner (19), but we are nevertheless left with this design.

The length of the chamber area is 45 feet, the antenna end (front) of the chamber is 16 feet wide while the back-wall of the chamber is 24 feet wide. The ceiling rises from a height of 14 feet at the front to
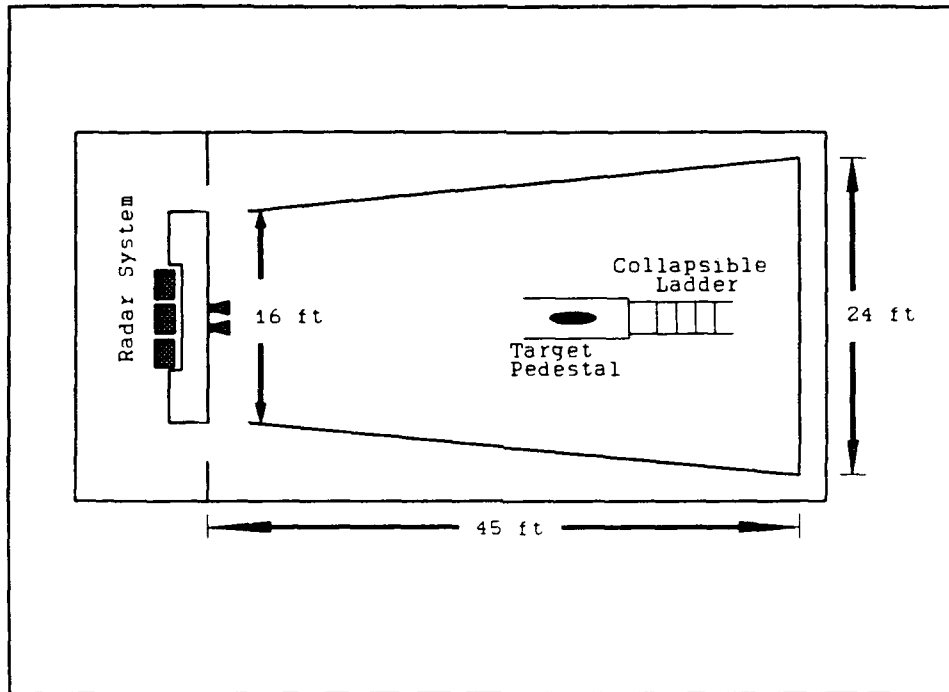
Figure 3.1   AFIT Anechoic Chamber, Plan View (12:9)

26 feet at the back-wall. There are two entrances located at the front

of the chamber on either side wall. Figure 3.2 shows an elevation view

of the chamber.

A target pedestal is located 26.5 feet from the front wall and is

centered in the cross-range dimension. The pedestal is designed to have

a low backscattered RCS, has the shape of a canted ogive cylinder, is

constructed of metal, and stands 7.5 feet high (see Figure 3.3). The

ogive cross-section and angle toward the radar antennas causes the

electromagnetic energy to be scattered from the pedestal in directions

other than the receive antenna or the target. The pedestal houses a

rotating turntable for mounting the target fixtures. The drive motor

and shaft for the turntable are contained within the pedestal.
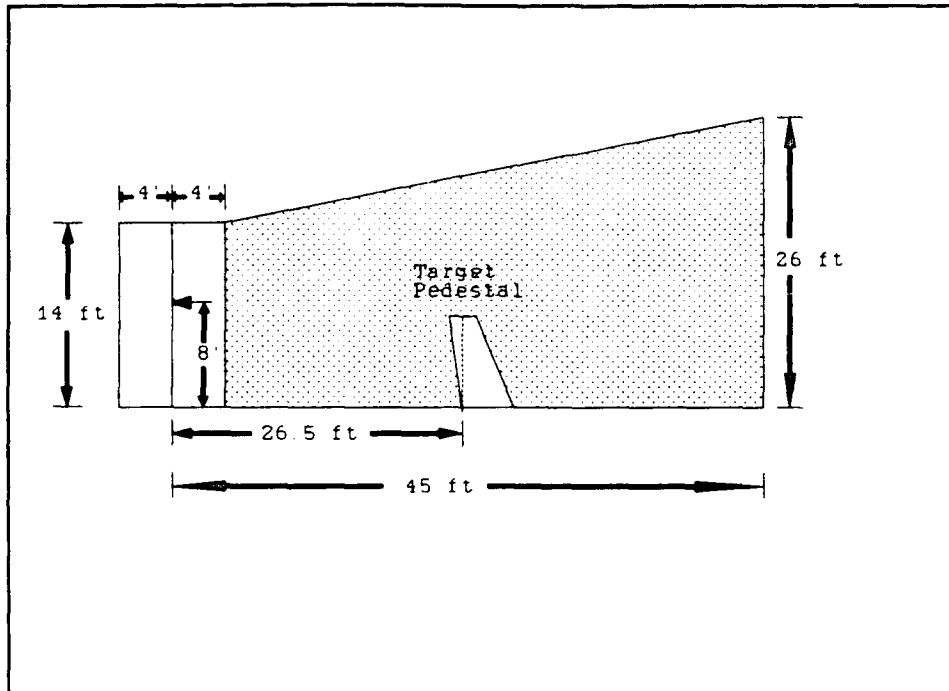
Figure 3.2 AFIT Anechoic Chamber Elevation View (12:10)

A folding wood and metal ladder allows access to the top of the pedestal for the mounting of target fixtures. This ladder has two arms that extend beyond the pedestal. These arm pivot on their respective mounts that are bolted to the chamber's concrete floor. The ladder it self has rubber wheels that allow it to travel along its guides which are two metal angles bolted to the floor. The base of the ladder locks into place when fully upright and provides for a stable platform from which to work. The assembly can be moved by a single person from its storage position of flat on the floor to its work position of just aft of the pedestal with minimum effort.

The radar transmits the electromagnetic energy into the chamber through a pyramidal horn antenna, the returned signal is received by an
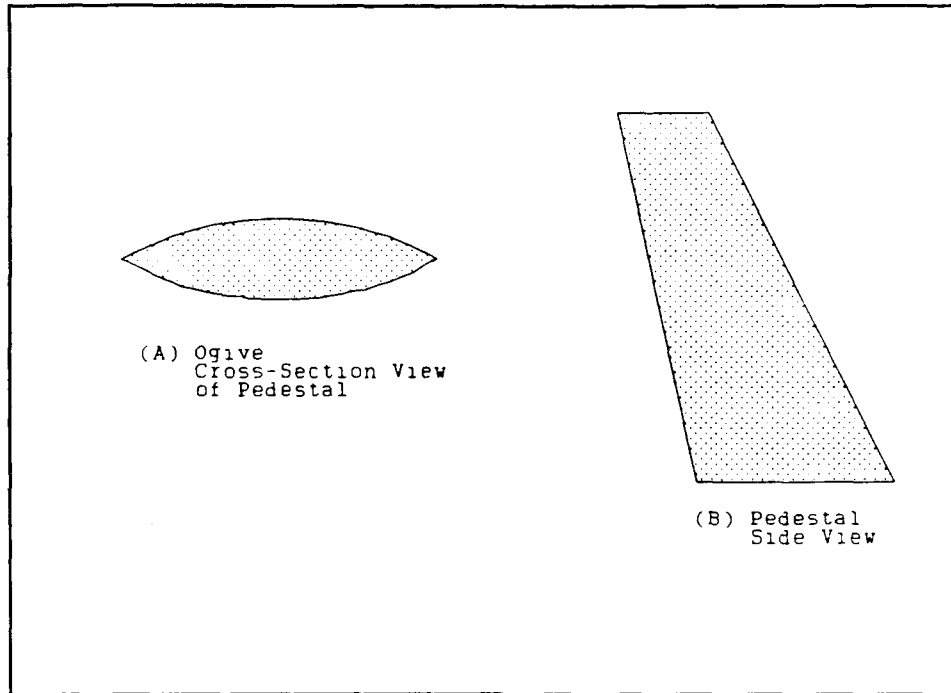
Figure 3.3 Target Pedestal, Cross-Section and Side View

identical antenna. The antennas are mounted adjacent to one another on

a rotating mount built into the front wall of the chamber. The antennas

are mounted in the "diamond" position, with adjacent corners of the two

antennas very nearly touching. The antennas are centered in the cross-

range dimension and are eight feet off the floor. The mounting fixture

allows the antennas to be rotated from one polarization to the other by

using a stepper motor controlled from the operations area.

The walls, ceiling, and most of the floor of the chamber are

covered with 18 inch pyramidal Radar Absorbing Material (RAM). The

floor area directly in front of the pedestal is covered with six inch

wedge RAM. The only portions of the chamber not covered with RAM are

the walk ways that allow access to the pedestal. Figure 3.4 shows a
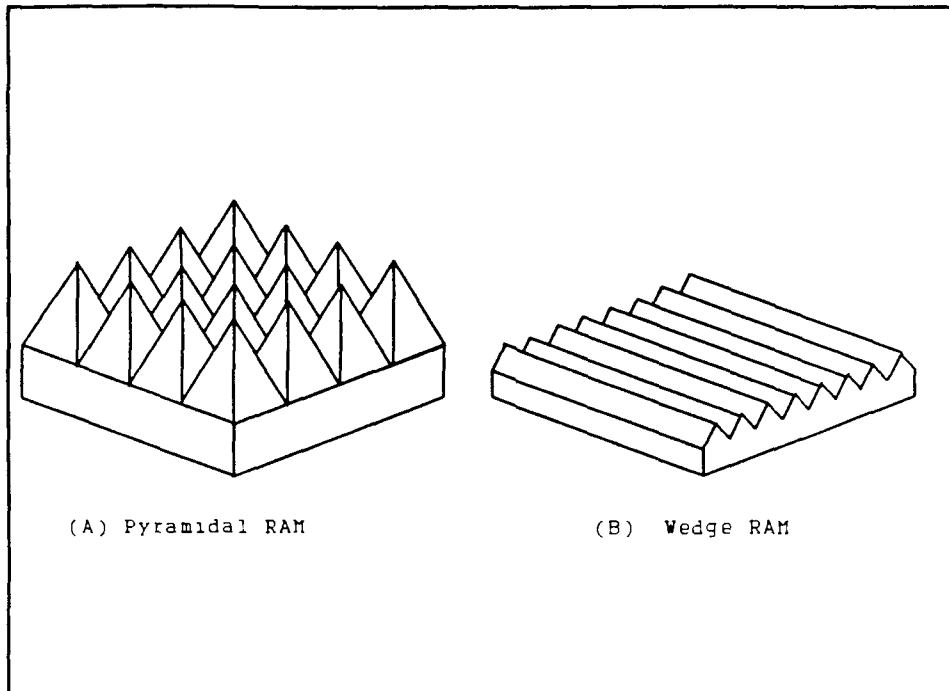
Figure 3.4 Pyramidal and Wedge Radar Absorbing Material
(RAM), adapted from (12:11)

block of both the pyramidal and wedge absorbers. The RAM is constructed

of carbon impregnated urethane foam. The 4'x4' blocks of pyramidal RAM

are glued to the conducting ceiling and walls of the chamber. The RAM

placed on the floor is unattached to allow free access to the chamber

floor space.

3.2 Radar System Hardware

This section describes the radar system hardware used to perform

RCS measurements in the AFIT anechoic chamber. A schematic of the

system is shown in Figure 3.5.

3.2.1 Source/Amplifier. The AFIT radar system transmi

continuous wave (CW) microwave frequencies generated by the HP 8340B
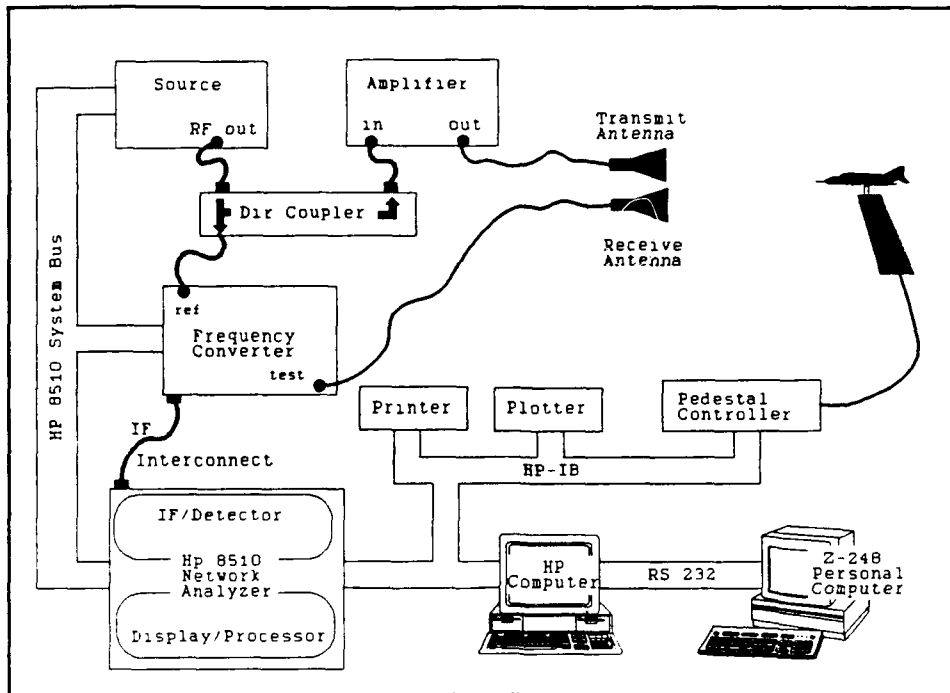
Figure 3.5   AFIT Radar System Schematic, adapted from (12:13)

Synthesized Sweeper.   The output of the sweeper is fixed at 0.0 dBm. The accuracy of the source for this output level is ±1.5 dB.   The output signal passes through a directional coupler and on to the HP 8349B Microwave Amplifier.   The amplifier boosts the signal to a fixed level of 24 dBm.   The amplifier stability for this low power output level is rated at ±1.25 dB.

   3.2.2 Antennas.   The antennas provide the transition between the coaxial feedlines from the amplifier to the free space of the anechoic chamber.   The antennas used are pyramidal horn antennas that have the special characteristic of their electric (E) field being oriented from corner to opposite corner of the horn.   Since the AFIT radar is a CW system two antennas are required, one to transmit the electromagnetic

signal and a second to receive the return signal. These antennas cover the frequency range of 6 GHz to 18 GHz. The main lobe of the antenna pattern provides very nearly plane wave illumination over a target zone that has the dimensions of 0.72 feet in both the vertical and horizontal planes, and 3.3 feet in the down-range direction (14:20).

3.2.3 Frequency Converter. The HP 8511A Frequency Converter functions to convert the RF test and reference signal to intermediate frequency (IF) of 20 MHz while preserving the relative amplitude and phase of the two signals. The IF signal from the HP8511A is passed to the HP 8510 Network Analyzer for measurement. This process of down converting the test and reference signals is not perfectly performed, but the calibration process will eliminate any frequency-dependent distortion introduced.

3.2.4 Network Analyzer. The HP 8510B Network Analyzer is the heart of the AFIT radar system. The HP 8510B is actually two pieces of hardware, the HP 85102 IF/Detector and the HP 85101 Display/Processor, that act in concert to form a single operating unit. The 20 MHz IF from the frequency converter enters the IF/Detector which down converts it to 150 KHz IF. It is here that the synchronous detectors determine the real and imaginary parts of the test signal relative to the reference signal. The relative phase and amplitude are sent to the Display/Processor for data processing and conversion to the display formats.

The HP 8510B may be operated manually from its front panel or by computer control via an HP Internal Bus (HP-IB). The source and

3-7

frequency converter are controller by the HP 8510B via the HP 8510 System Bus.

3.2.5 *Radar System Controller.* The AFIT radar system is controlled by an HP 9000 Series 236 Computer. The system is controlled through the HP-IB to the HP 8510 which in turn controls the source and frequency converter via the HP 8510 System Bus. The computer and network analyzer share the processing and calibration work load.

3.2.6 *Pedestal Controller.* The servo-mechanisms that rotate the target turntable (located in the top of the pedestal) and that reorient the antennas (for switching polarization) are controlled by a Newport Corporation 855C Controller. Antenna polarizations switching is manually entered into the handheld key pad, while the target turntable operation is directly controlled by the HP computer via the HP-IB.

3.2.7 *Peripherals.* Hard copy output of the RCS measurements is available from the HP 7470A Plotter. A print-out of the measurement software is available from an HP 2671G Printer. Both devices are connected to the computer via the HP-IB. The RCS measurement files may also be transferred to a Zenith 248 personal computer via an RS232 link. For the software written in (14) this data transfer is an off-line process. For this thesis the transfer to the Z-248 is the primary link to the data processing systems and is therefore an integral part of the data collection software.

3.3 Application to Imaging

In this section the application of the AFIT radar system for the purpose of radar imaging is discussed from both the general stepped CW point of view and specifically for the HP 8510 based system.

3.3.1 Stepped CW Application. (11) The Stepped CW radar is a relatively simple system that uses tunable, narrowband receivers synchronized to a programmable signal generator to provide a stepped frequency bandwidth for use in radar imaging applications. The narrowband receivers provide a high degree of amplitude sensitivity. However, the simplicity of the system comes at the cost of a high level of transmitter signal leakage to the receive antenna (antenna coupling) and a susceptibility to time-domain aliasing errors due to the discrete nature of the measured frequency response.

In the stepped CW system the transmitter leakage and other spurious signals received are frequency-dependent. Thus, to reduce the effects of these responses requires the use of post-detection cancellation. This entails the measurement of the chamber in the absence of the target and storing this information for later vector subtraction from the signals received with the target present. This is known as background subtraction.

Another concern is that of aliasing errors in the time domain, which may occur whenever the frequency response is collected at discrete frequency steps. Violation of the Nyquist sampling criterion may result in target responses in the time domain that will be indistinguishable from other undesired responses.

3-9

Both transmitter leakage and aliasing errors may be overcome by properly pulsing the transmitted signal and range gating the received signal. The receiver range gate effectively blocks the transmitter leakage and most of the undesired responses.

3.3.2 HP 8510 Based System. Currie presents several commercially available RCS measurement systems in Chapter 14 of his book, including the HP 8510 Network Analyzer based system (3:591-598). The ability of the HP 8510 to perform stepped frequency measurements is the primary feature that allows the system to be used in imaging applications. The stepped CW technique measures the target response at multiple frequencies over a band of interest. Vector subtraction is used to help remove spurious returns from the measurement environment and the range response of the target is determined by using the Fourier transform feature built into the HP 8510. The procedure just described yields the range profile of the target at a given aspect angle.

A system using the HP 8340 Synthesized Sweeper has an operating frequency range of 45 MHz to 26.5 GHz. The AFIT system uses this sweeper, but is band limited by the horn antennas which have a range of 6 GHz to 18 GHz. The operating frequency band is an important feature since range resolution is inversely proportional to the transmitted frequency bandwidth (see Equation 2.2). Operating at higher frequencies allows for greater bandwidth from a single signal generator and/or set of antennas. Of course, the actual frequency range used is governed by the frequencies at which one wants the frequency response and/or time response.

The HP 8510 performs stepped frequency measurements in either a ramp sweep or (synthesized) step sweep mode. Ramp sweep is the faster of the two modes. The synthesized step sweep mode is slower, since each measurement point requires 50 ms to synthesize the frequency. When averaging is used the two modes are comparable up to an averaging factor of about 128, after which the stepped sweep mode is significantly slowed. Averaging itself is a particularly useful feature since the system noise floor maybe reduced up to a factor of 10xlog(number of averages). This holds to a limit; it is related to receiver noise, clutter noise, source frequency stability and background subtraction.

3.4 *Existing Radar System Software* (14:21-42)

The purpose of this section is to review the existing radar system software. Emphasis will be placed on the portions of the code that were used as a basis for the two-dimensional image collection software written for this thesis effort (AFITIMAGE).

Overall control of the AFIT anechoic chamber radar system is handled by an HP 9236 computer by means of a software package called AFIT RCS Measurement Software (ARMS). The software package, which was written in HP Basic 3.0, automates the range instrumentation and interacts with the system operator to direct the measurement procedures. Calibration of raw data and vector background subtraction are performed by the software. Time domain post-processing is handled by the network analyzer.

The ARMS software has three major subroutines. The first performs frequency response measurements; this type of measurement is also known as a one-dimensional imaging or as a range profile, and thus this portion of the code is of primary importance to this thesis. The second major subroutine performs pattern cuts (RCS versus azimuth angle) and the third subroutine handles the processing and plotting of previously measured data. These last two subroutines will not be reviewed. Interested individuals are encouraged to read (14) for more details regarding these subroutines.

3.4.1 Calibration. Besides automating the radar instrumentation, the most significant purpose of the ARMS software is the calibration of the signal received from the target under test. This section explains the formula used in both the ARMS program and the AFITIMAGE program to produce calibrated RCS measurements of a target.

The definition of RCS, σ, is mathematically expressed as

$$\sigma = \lim_{R \to \infty} 4\pi R^2 \frac{|\mathbf{E}^s|^2}{|\mathbf{E}^i|^2} \tag{3.1}$$

where $\mathbf{E}^s$ (bold type indicates a vector) is the field scattered by the target, $\mathbf{E}^i$ is the field incident on the target, and R is the range from the antennas to the target. The limiting process in the definition assumes that we have plane wave incidence. The definition also assumes that our target is isolated in free space. In practice, R is made large enough so that the target illumination satisfactorily approximates a plane wave, and the target is mounted such that it will scatter as though isolated in space.

Let E^s_T represent the scattered field for our target; Equation 3.1 then tells us that if we know the quantity $(R\ E^s_T/E^i)$ we could find σ. However, with our target in place, the response of our radar system can be expressed as

$$K_1 E^s_T = K_2 (R\, E^s_T / E^i)$$ (3.2)

where K_1 is some complex constant that accounts for several system parameters (antenna gain, range, and so on), K_2 is the complex constant when R/E^i is factored out, and E^s_T is the scattered field of the target. Assume we also measure a (calibration) sphere, the system response to the sphere will be

$$K_2 (R\, E^s_S / E^i)$$ (3.3)

where K_2 is the same constant as in Equation 3.2, and E^s_S is the scattered field of the sphere. Assume we have calculated the quantity

$$(R\, E^s_S / E^i)$$ (3.4)

Finally, consider the following computation:

$$\frac{R E^s_S}{E^i} \frac{[\textit{Measured Target Response}]}{[\textit{Measured Sphere Response}]}$$

$$= \frac{R E^s_S}{E^i} \frac{K_2 R E^s_T / E^i}{K_2 R E^s_S / E^i}$$ (3.5)

$$= \frac{R E^s_T}{E^i}$$

Thus, it follows that

$$\sigma = 4\pi \frac{|RE_T^s|^2}{|E^i|^2} = 4\pi \frac{|RE_s^s|}{|E^i|} \frac{[Target\ Measurement]\ |^2}{[Sphere\ Measurement]\ |^2} \qquad (3.6)$$

The formula used by ARMS and AFITIMAGE takes one more step, called background subtraction, to provide "cleaner" target and sphere measurements. This is given by

$$\sigma = 4\pi \frac{|RE_s^s|}{|E^i|} \frac{[Target\ (Measurement-\ Background)]\ |^2}{[Sphere\ (Measurement-\ Background)]\ |^2} \qquad (3.7)$$

The accuracy of the RCS calculation will be dictated by the quality of the measured sphere and target returns. However, the background subtraction, no matter how accurate, can not account for the interactions between a measured object and the mounting fixtures, pedestal, or room. Note that the calibration equation developed above is applied at each individual frequency in the frequency response measurement.

3.4.2 Frequency Response Measurements. Frequency response measurements comprise one of the three major subroutines in the ARMS program. This type of measurement creates a one-dimensional image of an object. Portions of the code written for this subroutine are used in the AFITIMAGE program written for this thesis.

The frequency response measurement displays the RCS of an object as a function of frequency at a fixed aspect angle. The Fourier transform of an object's frequency response provides a bandlimited display of the object's response versus time. The object's bandlimited time response is an average of its response to the individual frequencies measurements. The network analyzer performs the Fourier

3-14

transform on the data and displays the trace of either the frequency

response or the time response on demand. The network analyzer, in

performing the four measurements required to obtain the frequency

response, samples the bandwidth of the sweep at 801 equally spaced

points. The real and imaginary parts of the complex return signal are

recorded in an 801 x 2 dimensioned array. Data averaging and a variable

range gate width are available through ARMS.

The ARMS program procedure for a frequency response measurement is

as follows: 1) The ARMS program obtains the following input information

from the operator: start and stop frequencies, antenna polarization,

range gate width, step sweep or ramp sweep mode for the frequency

generator, and the averaging factor. 2) The ARMS program directs the

operator to mount the appropriate mounting fixture, calibration sphere,

or target and collects the complex data from each of these measurements.

The first two measurements are of the calibration sphere and its column.

The complex data from these measurements are stored in arrays called

Reference and Ref_background. The last two measurements are of the

target mounting fixture and the target. The data form these

measurements are stored in arrays call Target_background and Target.

3) Upon completion of all measurements ARMS performs complex vector

background subtraction on the sphere and the target measurements. ARMS

reads in the calculation of the quantity $(R\ E^s_S/E^i)$ from a disk file and

performs the calibration of the frequency response as indicated in

Equation 3.7. 4) ARMS then sends the calibrated frequency response to

the network analyzer for display. The operator is given the choice of

3-15

viewing either the frequency response or the time response of the target. 5) Finally, ARMS stores the measurement to a disk file upon direction from the operator.

3.5 Summary

In this chapter the physical layout of the AFIT Anechoic Chamber presented. This was followed with a presentation of the radar hardware used in the AFIT chamber. The radar system was then evaluated for its application to the radar imaging process, both from a general stepped frequency CW viewpoint and from a hardware specific viewpoint. It was found in either case that the AFIT radar system can be used as presently configured for the purpose of radar imaging, but the operator must take precautions to ensure that aliased responses do not contaminate the data. Finally, portions of the existing radar system software called ARMS were reviewed. This review also included the development of the calibration equation used in both the ARMS software and in the AFITIMAGE software created for this thesis.

IV. AFIT Imaging Software

This chapter presents the software programs that collect and process the data for creating high resolution radar images. Two programs were developed during this thesis, one for data collection and another for data processing. The data collection program necessarily had to be considered first, and this used much of the time available for thesis study; thus, the data processing program is somewhat limited in its capabilities. The data collection program called AFITIMAGE was written in HP Basic 3.0 and runs on the HP 9000 Series 236 Computer that controls the AFIT Anechoic Chamber radar system. The data processing program, called AFIT Image Processing.M (AFITIP.M), was written using PC-MATLAB and runs on either a personal computer, such as the Z-248 installed in the anechoic chamber, or on the VAX computer system at AFIT. The AFITIMAGE program will be presented first with a general description of the program sequence. This will be followed by a description of the AFITIP.M program. The images created and the methodology used in validating the system will close the chapter.

4.1 Image Collection Software

The AFITIMAGE program borrowed significant portions of the ARMS software. This arises from the simple fact that the AFITIMAGE software automates what can be accomplished, with effort and time, through the ARMS software. In fact, prior to AFITIMAGE, the ARMS software was used

to "manually" collect an image data array, which was then processed interactively to prove the imaging capability. The array was collected using the existing ARMS software and transferred to the Z-248 for processing on a pc using PC-MATLAB. The collection of the data array required a separate frequency response measurement at each of the 32 aspect angles that made up the cross-range direction of the array. The 32 separate measurements were transferred to the Z-248 via the RS232 connection. The individual measurements and storage of files required 2.5 hours. The transfer of the files required 1.75 hours.

AFITIMAGE primarily acts to automate the data collection process. The program also checks the entered data collection specifications to ensure that the operator is attempting to collect good data. By reducing the amount of operator directed processes such as target movement, file storage, and file transfer much of the time involved in the data collection is eliminated.

The remainder of this section reviews the program AFITIMAGE in detail, addressing the decisions and logic behind the various sections. To assist the reader, a simplified flow chart has been included in the chapter, see Figure 4.1.

AFITIMAGE was written as an interactive program. Thus the program prompts the operator: for the image collection specification; to mount the sphere, target, and their respective columns; peak the target to establish a known aspect angle; and other operations. The program also displays data collection loop indicators that keep the operator informed of the collection process.

```
┌─────────────────────────┐
│ Enter Data Collection   │
│ Specifications          │
└─────────────────────────┘
            │
            ▼
┌─────────────────────────┐
│ Measure and Store       │
│ Sphere Background        │
│ Sphere                  │
│ Target Background       │
└─────────────────────────┘
            │
            ▼
┌─────────────────────────────────┐
│         Peak the Target         │
│ (Align to a known aspect angle) │
└─────────────────────────────────┘
            │
            ▼
┌──────────────────────────────────────┐
│ Move Target to First Collection Angle │
└──────────────────────────────────────┘
            │
            ▼ ◄─────────────────────────┐
┌─────────────────────────┐            │
│ Collect the Frequency   │            │
│ Responce of the Target  │            │
└─────────────────────────┘            │
            │                          │
            ▼                          │
┌─────────────────────────┐            │
│ Calculate the Calibrated│            │
│ RCS of the Target       │            │
│      and                │            │
│ Store as One Column of  │            │
│ the Data Array          │            │
└─────────────────────────┘            │
            │                          │
            ▼                          │
┌─────────────────────────┐            │
│ Move to the             │            │
│ Next Data               │            │
│ Collection Angle        │            │
└─────────────────────────┘            │
            │                          │
            ▼                          │
          ╱────╲                       │
        ╱        ╲                     │
      ╱  Done  ?   ╲───────────────────┘
        ╲        ╱
          ╲────╱
            │
            ▼
┌──────────────────────────────────┐
│ Transfer Array to the Z-248      │
└──────────────────────────────────┘
```

Figure 4.1 Simplified Flow Chart of AFITIMAGE

Upon program initiation the operator is asked to enter the current date. This information will be stored in the array header (the first column of the data array) for use during post-processing. The main menu for program direction is then displayed. The operator may choose from the following soft-key options:

K0 - Enter image collection specifications. Chosen if making an initial pass through the collection process. All the image collection specifications are entered with this choice.

K2 - Choose a new angle. After the first array is collected and transferred a second array may be collected with a different set of aspect angles. This is a time saver since only the target is measured.

K4 - Transfer the array to Z-248. The transfer of the array to the Z-248 is the only means of post-processing the array at this time. Thus the transfer of the array is an integral part of the data collection program.

K6 - Back to BASIC. Normal program termination; the program allows the operator to return to the program to transfer data if the key was inadvertently struck.

When K0-Enter image collection specifications is selected, the next several computer screens are used to prompt the operator for data collection specifications. The general form is for the program to request a specification entry, while also displaying the present value and, if one exists, the default value of the variable. If the operator hits ENTER then the default value, or present value if there is no

default, is taken as the value of the variable. This format allows the operator to see the previously entered values. This feature is extremely useful if the operator decides to change the entries upon viewing the entire listing of the entered values. The data specification entries are: the start and stop frequencies; the antenna polarization; the averaging factor to be used (any power of two between 1 and 4096 with 32 as the default); the time gate (seven nano-seconds is the default); the number of data samples in the frequency direction (any number between 32 and 401, with a power of two suggested, and a default of 128); the target's longest horizontal dimension (used in determining if the data sampling is correct); start and stop angle (any angle ± 360°, as long as the start angle is smaller than the stop angle); the number of samples in the angle direction (a power of two is suggested, with a default of 32). As the various specifications are entered the program checks to ensure that an allowable value was entered. If an illegal value is entered, the program loops back until an allowable value is entered.

After all the specifications have been entered, the program checks to insure that the Nyquist sampling criterion is satisfied for both the frequency and angle directions. The program also checks the total data collection angle to determine if the resulting image will require focusing to correct for the migration of scatterers through resolution cells. The program warns the operator if any of these checks fail, but the operator can choose to ignore these warnings.

Before starting the data collection, the program displays the specifications entered by the operator and the calculated cell sizes. The operator is allowed to change the entries by looping back to the first line of entry code. This forces the operator to enter all the specifications again, but by having the present value of the specification displayed the operation is greatly simplified.

If the new angle option (K2) had been chosen the only data specifications required would be the start angle, stop angle, and number of angle samples. All other data specifications would remain the same as on the first data collection.

The network analyzer is set up for data collection using the frequency list mode option. The frequency list mode, a variation of the step sweep mode, synthesizes each of the transmitted frequencies. By synthesizing the individual frequencies, the averaging of multiple measurements to reduce the system noise is enhanced since the frequencies are precisely repeated. The frequency list option allows the operator to select any number of data samples from 1 to 401. This capability is considered useful, as compared to either the ramp sweep or step sweep mode, where the number of data samples is limited to the values of 51, 101, 201, 401, and 801. Prior to the network analyzer initialization the program has checked to ensure that the frequency step size allows for an aliasing range greater than the furthest target dimension. Beyond the aliasing requirement is the need to correctly capture the characteristics of the returned waveform, thus over-sampling of the frequency response is generally recommended.

After initializing the network analyzer, the program displays, in turn, the first three mounting headers. These headers instruct the operator to mount either the sphere column, the sphere, or the target column. After each of these items has been mounted, the operator commands the program to make a measurement. Each of these measurements are stored in an array for later processing by the computer.

Before the target can be measured, it is necessary to establish a known aspect angle on the target. To do this, the program initializes the turntable controller and the network analyzer is placed in a continual ramp sweep mode. This allows these two pieces of equipment to be used by the operator to peak the target return at some known aspect angle. All the instructions that a novice operator needs to accomplish this task are presented by the program using the target mounting header. The procedure is a rather simple one in which the operator, after mounting the target at some unknown aspect relative to the radar, can use the handheld keypad of the controller or the front arrow keys to move the target through a range of angles. By monitoring the network analyzer display the operator can determine when the target return signal reaches a peak value. This peak value is associated with some known high return area such as broadside to an aircraft. The operator enters this known value into the controller keypad and returns control of the controller to the computer.

Once the known aspect angle has been entered into the controller the computer commands the controller to move the target to the first data collection angle. Since this operation may require either no time

at all or up to several seconds, the operator is prompted to instruct the computer to start the measurement process after the target has reached the first data collection angle.

The target measurement sequence is contained in a program loop. For each pass through this loop the target is measured, the calibrated frequency response is calculated (see Section 3.4.1 for a description of this calculation), the frequency response is stored as one column of the data array, and the target moves to the next measurement angle. While the computer is calculating and storing the data the target is moving to the next measurement location. During the entire process the computer screen displays a message telling the operator which of the data collection points is presently being processed. After the frequency response for each angular increment has been collected, the image collection specifications are stored in the first column of the array. This header information remains with the array during the post-processing sequence so that all the information necessary to repeat the measurement is available with the image produced by the data process ing program.

The operator is informed that the data collection sequence is complete and the program warns the operator to transfer the image array, else the data will be lost. The program then returns to the main menu for choice of the next option selection.

When the K4-Transfer to Z-248 option is selected, the program transfers the collected image array from the computer memory to the

4-8

Z-248 via an RS232 port. The program displays a message instructing the operator on the setup of the Z-248 for the data transfer. After completing the setup actions, the operator commands the program to start the data transfer. The image array is transferred as one continuous column of data. The data processing program will return the array to columns of real and imaginary pairs.

When the operator selects the K6-Back to BASIC option the program terminates after allowing the operator the opportunity of returning to the program to transfer data.

4.2 Image Processing Software

The image processing software called AFITIP.M was written using PC-MATLAB software. A MATLAB M-file is a collection of MATLAB commands that are stored as a file, in this regard an M-file is similar to a DOS batch file. AFITIP.M is an interactive program that allows the operator to direct certain of the processing operations. The software can run on any MS-DOS based computer that is equipped with a math co-processor. There is also a main-frame version of this software called PRO-MATLAB that runs on the VAX computer system at AFIT. The major drawback of the PC version is the array size limitation of 8192 elements. Since each of the image data array elements is complex, this limitation equates to an array of roughly 128 rows x 32 columns. The array is required to be 2^mx2^n since FFTs are used to process the array. If the collected array is not 2^mx2^n, the program zero pads the array to the next larger power of two in each direction.

```
┌─────────────────────────────┐
│   Translate Array to        │
│   MATLAB Format             │
└─────────────────────────────┘
              │
              ▼
┌─────────────────────────────┐
│      Strip Header           │
│         and                 │
│   Reconstruct Array         │
└─────────────────────────────┘
              │
              ▼
┌─────────────────────────────┐
│     Choose Window           │
│         and                 │
│   Window the Array          │
└─────────────────────────────┘
              │
              ▼
┌─────────────────────────────┐
│   Zero pad the Array        │
└─────────────────────────────┘
              │
              ▼
┌─────────────────────────────┐
│   Apply 2-D IFFT            │
└─────────────────────────────┘
              │
              ▼
┌─────────────────────────────┐
│   20xlog(magnitude) of the  │
│   Array Elements            │
└─────────────────────────────┘
              │
              ▼
┌─────────────────────────────┐
│   Display the Image         │
└─────────────────────────────┘
              │
              ▼
┌─────────────────────────────┐
│   Store the Array           │
└─────────────────────────────┘
              │
              ▼
┌─────────────────────────────┐
│      Demonstrate            │
│   Array manipulation and    │
│   display features          │
└─────────────────────────────┘
              │
              ▼
┌─────────────────────────────┐
│   Program Ends Allowing     │
│   Operator to find Best View│
│   and Print Results         │
└─────────────────────────────┘
```
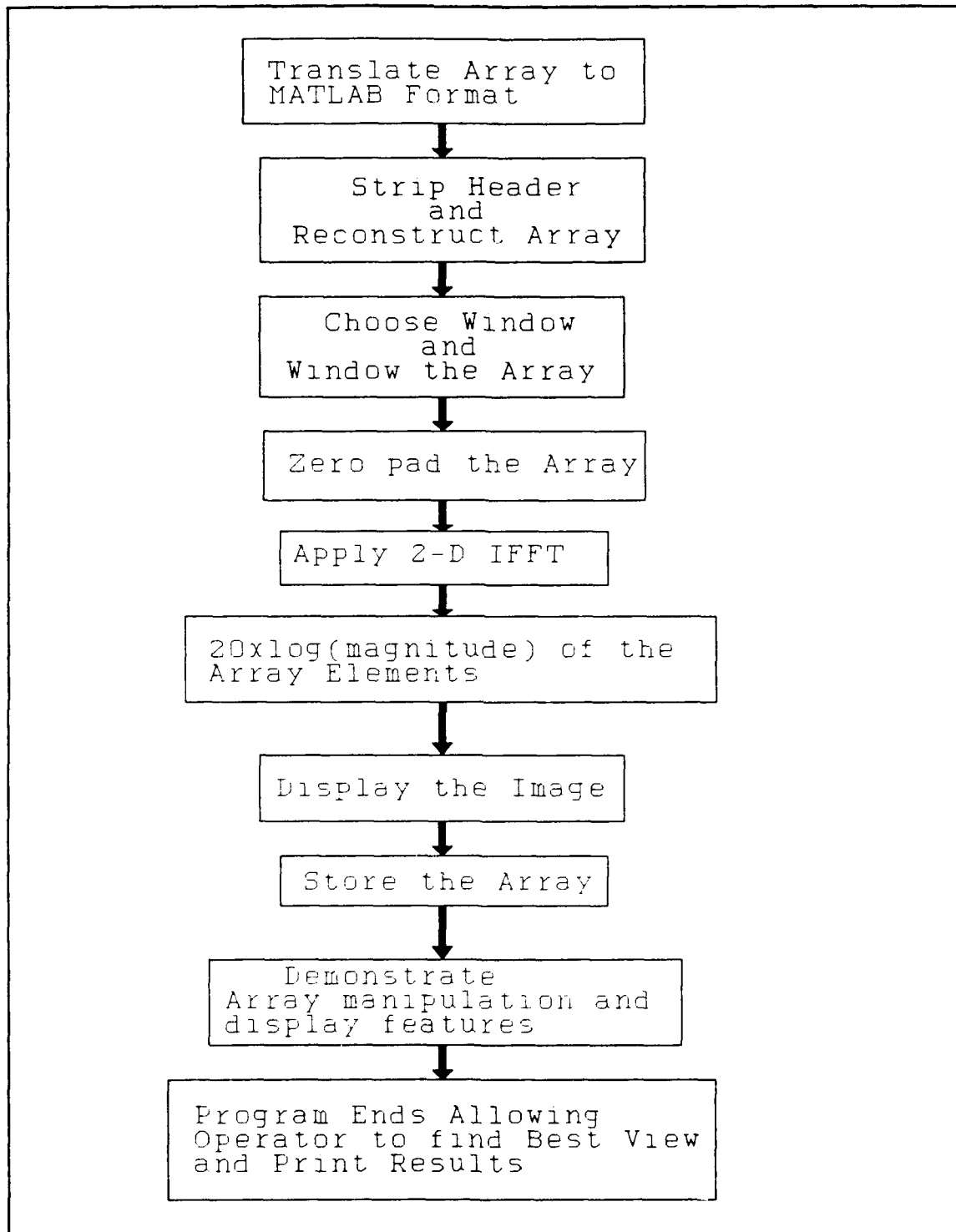
Figure 4.2   Simplified Flow Chart of AFITIP.M

MATLAB (which stands for matrix laboratory) is an integrated system; this means that programmable macros, IEEE arithmetic, analytical commands, and graphics are all included in the system. MATLAB has an on-line help function that handles most of the questions that arise in using the system (13:3-4).

AFITIP.M automates the data processing operations that the operator would otherwise have entered by hand, to obtain a high resolution radar image from the data collected using the AFITIMAGE program. AFITIP.M displays most of the equations that are used to perform the processing and informs the operator of each step taken in the processing sequence. The program, which is stored as a DOS text file, may be read by any word processing system and a printout may be obtained for detailed review.

On machines that already have a version of MATLAB installed and the AFITIP.M file in the directory, the operator starts the data processing sequence by entering AFITIP at the MATLAB prompt. The operator is greeted to the AFIT image processing software and told that the first operation is the translation of the ASCII data file, obtained in the data transfer operation using AFITIMAGE, into the MATLAB format. The operator is given the answers to the questions presented by the translation program. By answering the question in the specified manner the data array is assigned a specific name that is used during the data processing.

After the data has been read into MATLAB, the program must strip off the header information and reconstruct the data collection array

into columns of real and imaginary pairs. The header contains all the data collection specifications and is used in processing the data as well as providing the information necessary to repeat the measurement.

It was found that the IFFT of each of the collected frequency response measurements would produce an image with the target occupying only a very small portion of the center of the image. The processing reduces the number of frequency data points in the array by a factor of 10, this spreads the target to fill the image plane.

Once the array has been reduced, the next operation is to window the array to minimize the processing sidelobes that occur when taking the Fourier transform of a truncated data set (see Section 2.5.2 for more information). The operator is given a choice of six windows that may be applied: rectangular (no window); triangular; Hanning (cosine squared); Hamming; Blackman; and Bartlett. Displayed along with the windows are their highest sidelobe level and the resolution cell size spreading factor. The highest sidelobe levels are -13 dB, -27 dB, -32 dB, -43 dB, and -51 dB, respectively (6:55). As mentioned in Section 2.5.2, the use of windows minimizes the processing sidelobes at the expense of increasing the resolution cell size. The resolution cell size spreading factor was calculated from the 3 dB bandwidths of the central spike of each window as given by Harris (6:55). Since the rectangular window is effectively no window, its 3 dB bandwidth is the narrowest that can be achieved. All other windows will have a wider 3 dB bandwidth and thus an increased resolution cell size. The resolution cell size spreading factor is calculated by dividing the 3 dB bandwidth

of the given window by the 3 dB of the rectangular window. These
values, for the first five windows, are 1.00, 1.43, 1.62, 1.46, and 1.71
respectively. The value calculated in this manner for the Hamming
window, 1.46, agrees well with the value given by Currie of 1.47
(3:385). Harris did not evaluate the Bartlett window, thus information
on the 3 dB bandwidth and spreading factor is unavailable.

The next step is to zero pad the array to obtain a $2^m \times 2^n$ array.
This step is necessary if the FFT algorithms are to be used. MATLAB
would zero pad the array itself, but it does so by tacking the zeros on
to the end of the matrix. It is desired to equally pad the data matrix
with zeros on either side. If the array is already a $2^m \times 2^n$ array, the
array will not be padded.

The windowed,padded array is then processed by a two-dimensional
IFFT. After applying the two-dimensional IFFT, it is necessary to shift
the array to compensate for the fold-over that occurs with the Fourier
transform. This step is accomplished by using another one of MATLABs
built in functions. This processing will produce the complex data for
the reflectivity distribution map of the target. To obtain the standard
RCS image from this data, the program must compute the 20xlog(magnitude)
of each element in the array.

After this last processing step, the image is displayed with the
range and cross-range directions shown on the axis. The operator is
instructed to rename the array and save it for possible future
processing. The last section of the program demonstrates to the
operator how the low level "noise" can be removed by setting a lower

bound on the data. This last step is accomplished using another M-file that produces the desired results given the data array , the array size, and the minimum value desired. The operator is shown how to enter the titles and the axis labels for the array by having the operator enter this data on their own for the image. Finally, the operator is instructed on obtaining a printout of the image. This ends the active processing by the program and the operator is returned to the MATLAB system to find the best set of viewing angles of the image.

4.3 *System Validation*

The AFITIMAGE software was validated in all of its subroutines by verifying that each portion of the program performed as intended. After each subroutine was validated, the whole system was exercised by collection an image array of a six inch sphere. The processed range profile generated was sent back to the HP 8510 for time domain processing. The bandlimited time domain plots from the AFITIMAGE program overlaid those produced by the ARMS program.

The next step in validating the system was to collect image data of three right circular cylinders 2.54 centimeters in diameter by 7.64 centimeters in length on a styrofoam column (see Figure 4.3). The columns were measured at three angles: 0°, 45°, and 90°. All measurements cover the frequency range of 14 to 18 GHz and use a vertically polarized E-field. Thirty two individual measurements were averaged at each frequency point by the HP8510. A time gate of 7 nanoseconds was used to gate out undesired chamber signals. Two hundred
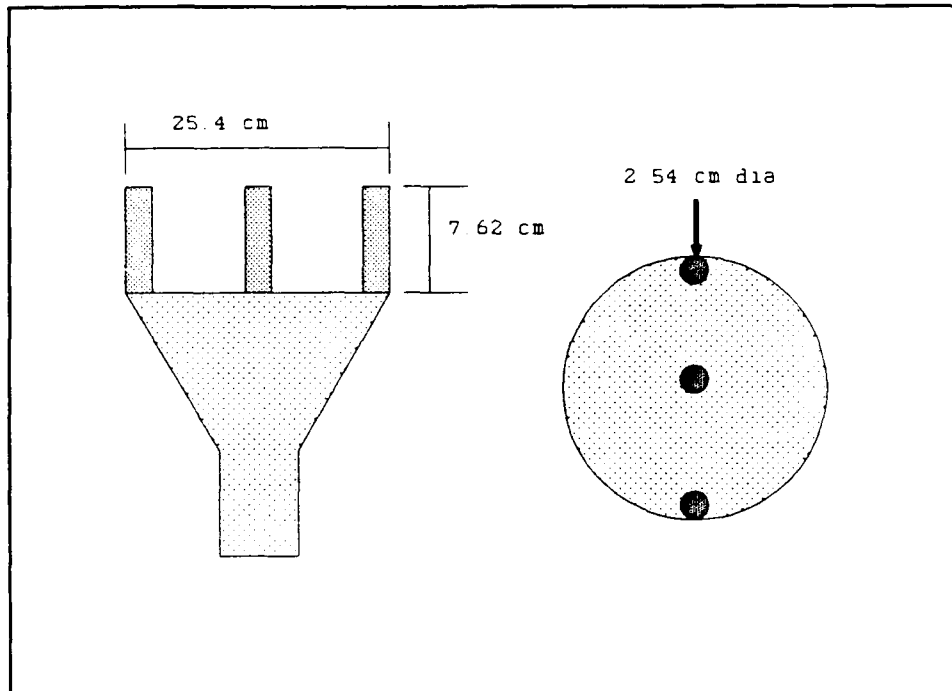
Figure 4.3 Validation Target

forty frequency samples were collected over this band. Of the 240

samples collected, 24 were used to create the images. This reduction is

performed to expand the target zone to occupy the full image display

area. The target was measured at 16 different angles over a $\Delta\theta$ of

14.5°. The cylinders were aligned in a straight line on the top of a

foam column 25.4 centimeters in diameter. These specifications provided

a range resolution of 3.75 centimeter and a cross-range resolution of

3.74 centimeters.

The collected data arrays were processed using the AFITIP.M macro

written for use with the PC-MATLAB software. As can be seen in Figures

4.4 - 4.6, the images produced are rather course. This is due to the

limited number of data points in the array used to produce the images.

Despite this coarseness the three cylinders are clearly visible in all three of the contour plots. Figure 4.6a and b exhibit three small peaks directly behind the three cylinders. Since vertical polarization was used to collect the data these features cannot be the creeping wave response of the cylinders. Similar features are seen in the other images as well. The relatively low clutter ahead of the columns is most likely for the foam column support. This column was part of the "fixed" background that was subtracted from the target data, but since the target support is only measured at one azimuth angle its contribution to the target measurement can not be fully background subtracted. As can be seen in Figure 4.4b, the foam column background is subtracted almost completely. This is due to the fact that the target background was measured at zero degrees azimuth angle.

4.4 *Summary*

The collection software, AFITIMAGE, provides the data necessary for the production of ISAR images. AFITIMAGE provides several parameters that are under the control of the operator that influence the resulting images. The agreement between the individual range measurements made using AFITIMAGE and the ARMS software provide confidence in the validity of its processing and algorithms.

The data processing software, AFITIP.M, is a first cut solution to the task of producing images from the data collected using AFITIMAGE. The unanticipated necessity of reducing the frequency samples to produce images that occupy the entire time space is still not fully understood.

(A) Waterfall Plot of Three Cylinders at 0 Degrees

Cross-Range

Down-Range

(B) Contour Plot of Three Cylinders at 0 Degrees

Cross-Range

Down-Range
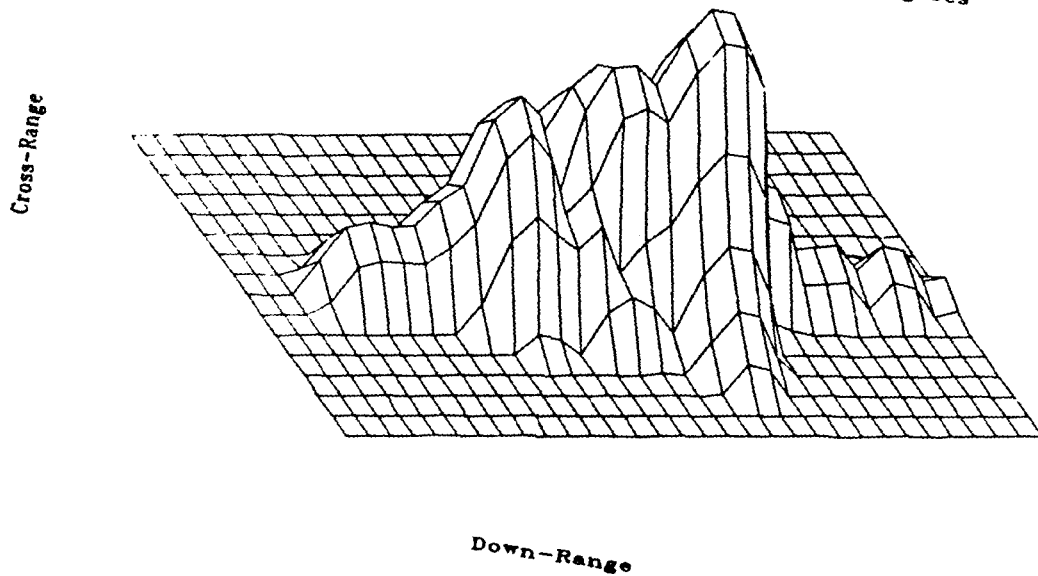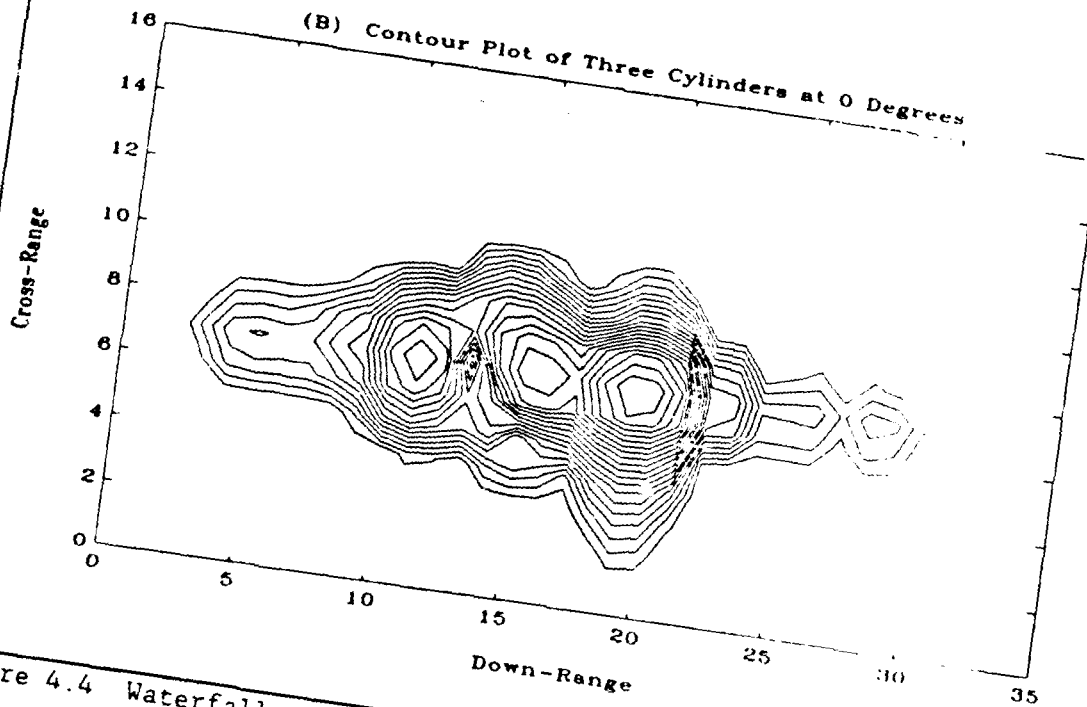
Figure 4.4 Waterfall and Contour Plots of Three Cylinders at 0°

4-17

(A) Waterfall Plot of Three Cylinders at 45 Degrees

Cross-Range

Down-Range

(B) Contour Plot of Three Cylinders at 45 Degrees

Cross-Range

Down-Range
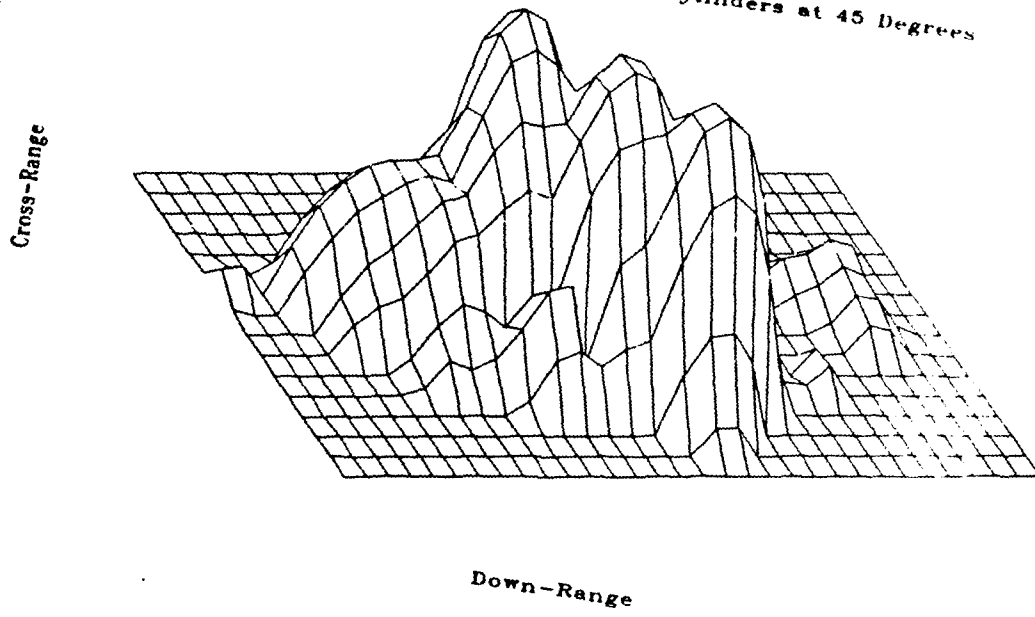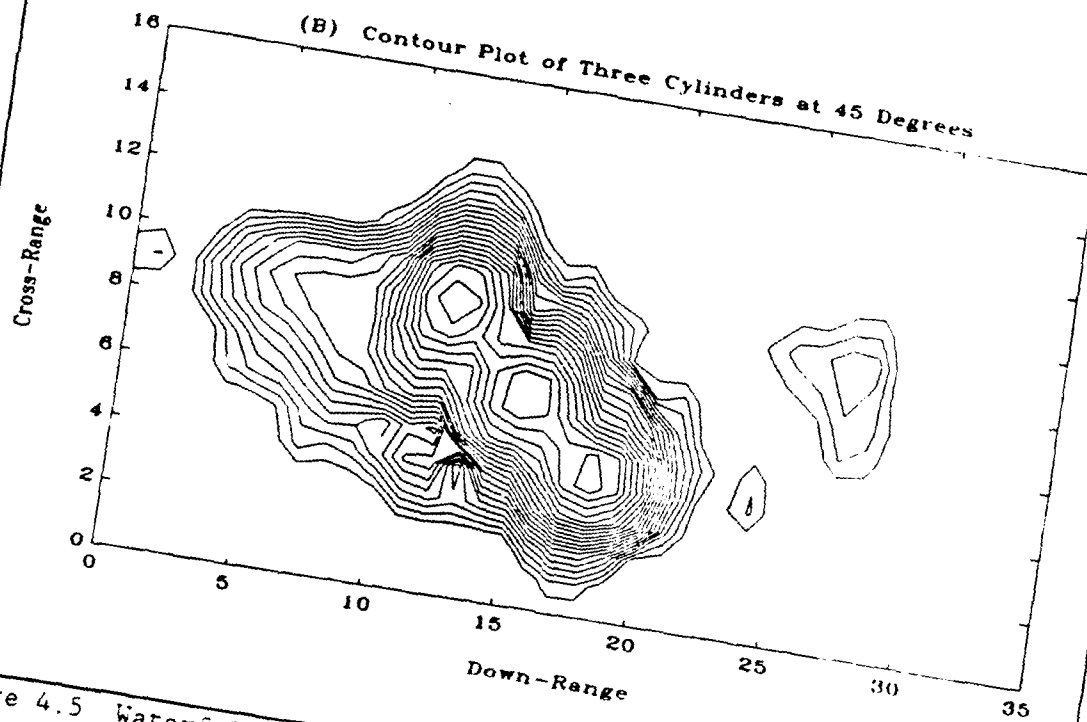
Figure 4.5 Waterfall and Contour Plots of Three Cylinders at 45°

4-18

(A) Waterfall Plot of Three Cylinders at 90 Degrees

Down-Range

(B) Contour Plot of Three Cylinders at 90 Degrees

Down-Range

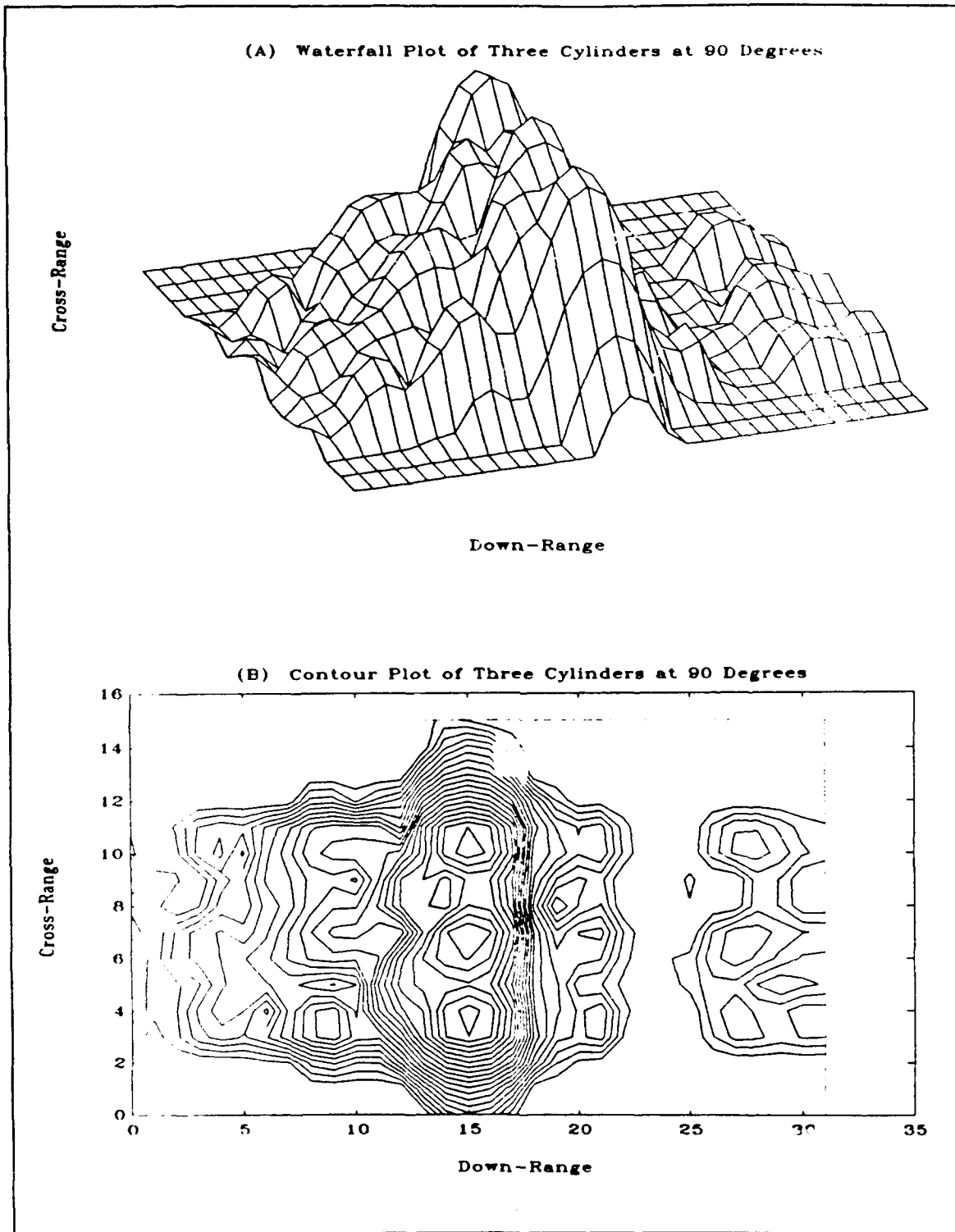Figure 4.6 Waterfall and Contour Plots of Three Cylinders at 90°

It was also found that the IFFT produced results that were reduced in peak power from that observed using the ARMS software for a similar target. There is some indication that this may be attributable to the zero padding of the array needed for the FFT algorithms. A possible solution may be to average pad the array before the two-dimensional window is applied.

V. Conclusions and Recommendations

The problem statement for this thesis was to develop an ISAR imaging capability for the AFIT anechoic chamber. To accomplish this task required the development of two software programs one for data collection and a second for data processing. Each of these software packages will be addressed individually.

5.1 Data Collection Software

It was learned early in the thesis process that the data collection software would receive the majority of the time and effort available for this thesis. Thus, the AFITIMAGE software developed for the data collection is a flexible tool that may be used by the faculty and students at AFIT to study the area of high resolution radar imaging. As indicated in Chapter 4, the software is capable of collecting data over any segment of the bandwidth available with the AFIT radar system. Any number of data points may be collected in either the frequency or angle directions, including values that violate the Nyquist sampling criterion. The software algorithms are based on those developed for the ARMS software. Thus, there is a continuity between the radar measurement programs that will facilitate any future developments or improvements to either software package.

The AFITIMAGE software might be improved by using the HP 8510 to perform the complex vector mathematics required in obtaining calibrated

measurements. The background subtraction of both the calibration sphere and the target may be accomplished by storing each of the background measurements in the memory of the network analyzer. The sphere (target) would then be measured and the stored background subtracted from the data. If the sphere minus background and target minus background measurements are stored in the network analyzer memory they can be divided. The resulting array answer from these math operations would then be transferred to the HP 9000 series computer for final processing to obtain a calibrated measurement. Using this process should improve the processing efficiency since the ᴾasic 3.0 code that runs on the HP 9000 series computer can not handle complex arithmetic and the HP 9000 computer is rather slow compared to the HP 8510.

The whole area of bistatic imaging is also available for investigation. Whether this would require a separate program or could be incorporated into the existing code is unknown.

The radar system could be improved for imaging purposes by adding a hardware range-gate and pulsing the transmitted signal. As mentioned in Section 3.3, this would eliminate the disadvantages associated with stepped CW radar systems.

5.2 Data Processing Software

Since most of the time and effort associated with this thesis was concentrated in obtaining a very capable data collection software package, the data processing software is limited in its capability. The software does automate the processing involved in obtaining radar

images, while providing some capability in regards to: studying the effects of the various window applications on the image resolution; elimination of low-level "noise" from the image, thus enhancing the target characteristics; and manipulation of the image display to achieve an optimum display of the target characteristics.

Although the software is capable of performing most of the processing required to obtain a high resolution image, its inability to perform image focu_ing ultimately limits the level of resolution that may be obtained (see Section 2.4.1). Thus the major recommended improvement for this software is the inclusion of image focusing algorithms.

Other interesting and valuable capabilities that might be included in an improved software package would be: image editing; range and cross-range profiles; image zooming; and mixed processing. Image editing would allow the selective elimination of spurious returns that show up in an image. These returns generally take the form of stationary clutter that shows up on the center line of the image. The range and cross-range profiles are readily available from the data matrix. By specifying, possibly with a cursor, the intersection of a range and cross-range line on the image, the associated range and cross-range profiles could be displayed in separate windows or possibly separate plots. Image zooming would allow the operator to blow up a given portion of the image array for closer examination. Mixed processing is the ability to overlay several images from different aspect angles to obtain a composite image of the target.

Bibliography

1. Ausherman, Dale A. et al. "Developments in Radar Imaging," *IEEE Transactions on Aerospace and Electronic Systems, Volume AES-20, Number 4*: 363-400 (July 1984).

2. Brown, William M. and Ronald J. Fredricks. "Range-Doppler Imaging with Motion Through Resolution Cells," *IEEE Transactions on Aerospace and Electronic Systems, Volume AES-5, Number 1*: 98-102 (January 1969).

3. Currie, Nicholas C., editor. *Radar Reflectivity Measurement: Techniques and Applications*. Artech House, Norwood MA, 1989.

4. Gabriel W.F. "Superresolution Techniques and ISAR Imaging," *Proceedings of the 1989 National Radar Conference*. 48-55. New York: IEEE Press, 1989.

5. Halevy, S. et al. "Efficient Range-Doppler Imaging of Rotating Targets," *Proceedings of the 1984 National Radar Conference*. 53-57. New York: IEEE Press, 1984.

6. Harris, Fredric J. "On the Use of Windows for Harmonic Analysis with the Discrete Fourier Transform," *Proceedings of the IEEE, Volume 66, Number 1*: 51-83 (January 1978).

7. Jay, F. *IEEE Standard Dictionary of Electrical and Electronics Terms*. IEEE Inc., New York, 1977.

8. Joseph, Capt Philip J. *A UTD Scattering Analysis of Pyramidal Absorber For Design of Compact Range Chambers*. PhD dissertation. The Ohio State University, Columbus OH, 1988.

9. Mather, Bruce C. *Fourier Domain Interpolation Techniques for Synthetic Aperture Radar*. PhD dissertation. University of Illinois at Urbana-Champaign, Urbana IL, 1986 (AD-A170983) (UILU-ENG-86-2226).

10. Mensa, Dean L. *High Resolution Radar Imaging*. Dedham MA: Artech House, Inc., 1984.

11. ------. Lecture Notes distributed in Engineering 867.80, High-Resolution Radar Cross Section Imaging. University of California, Los Angeles; University Extension, Department of Engineering and Science Short Course Programs; Los Angeles CA, January 19-21 1988.

12. Mensa, Dean L. and K. Vaccaro. "Two-Dimensional RCS Image Focusing," *Proceedings of 1987 Meeting of the Antenna Measurement Techniques Association*

13. Moler, Cleve et al. *PC-MATLAB User's Guide*. Sherborn, MA: The Math Works, Inc., 1987.

14. Owens, Capt Scott A. *Automation of an RCS Measurement System and Its Application to Investigate the Electromagnetic Scattering from Scale Model Aircraft Canopies*. MS thesis, AFIT/GE/ENG/89D-38. School of Engineering, Air Force Institute of Technology (AU), Wright-Patterson AFB OH, December 1989 (AD-A215-741).

15. Prickett, M. J. and C. C. Chen. "Principles of Inverse Synthetic Aperture Radar (ISAR) Imaging," *IEEE Electronics and Aerospace Systems Conference*. 340-345. New York: IEEE Press, 1980.

16. Reedy, E.K. et al. "Three-Dimensional Imaging of Radar Targets at 95 GHz," *Proceedings of the 1986 IEEE National Radar Conference*. 7-11. New York: IEEE Press, 1986.

17. Skolnik, Merrill I., editor. *Introduction to Radar Systems* (Second Edition). New York: McGraw-Hill, Inc., 1980.

18. Steinberg, Bernard D. et al. "Experimental Localized Radar Cross Sections of Aircraft," *Proceedings of the IEEE, Volume 77, Number 5*: 663-669 (May 1989).

19. Swarner, W.G. et al., Sixth Status Report on Contract #OR-549651-B28, ElectorScience Laboratory, The Ohio State University, Columbus OH.

20. Walker, Jack L. "Range-Doppler Imaging of Rotating Objects," *IEEE Transactions on Aerospace and Electronic Systems, Volume AES-16, Number 1*: 23-52 (January 1980).

21. Wehner, Donald R. *High Resolution Radar*. Dedham, MA: Artech House, Inc., 1987.

Vita

Captain Brian K. Sanders was born in Festus Missouri, on 23 June 1958. He graduated from Fox Senior High School in Arnold, Missouri in 1976. Captain Sanders enlisted in the Air Force in December 1981 in the Electronic Warfare Maintenance career field. In June of 1983 he was selected for the Airmen's Education and Commissioning Program and received his Bachelor of Science degree in Electrical Engineering from the University of Missouri at Columbia in December 1985. Captain Sanders received his commission at the USAF Officer Training School in April 1986. His first assignment as an officer was to the Radar Target Scatter (RATSCAT) division of the 6585th Test Group at Holloman AFB, New Mexico. Captain Sanders worked as a site engineer at the RATSCAT Advanced Measurement System (RAMS) facility from April 1986 to December 1987. From December 1987 till entering the School of Engineering, Air Force Institute of Technology, in May 1989 Captain Sanders was an RCS Test Manager at the RATSCAT Mainsite facility.

Permanent address: 42 Sandiscott Dr

Arnold, MO 63010

REPORT DOCUMENTATION PAGE

Public reporting burden for this collection of information is estimated to average 1 hour per response, including the time for reviewing instructions, searching existing data sources, gathering and maintaining the data needed, and completing and reviewing the collection of information. Send comments regarding this burden estimate or any other aspect of this collection of information, including suggestions for reducing this burden, to Washington Headquarters Services, Directorate for Information Operations and Reports, 1215 Jefferson Davis Highway, Suite 1204, Arlington, VA 22202-4302, and to the Office of Management and Budget, Paperwork Reduction Project (0704-0188), Washington, DC 20503.

1. AGENCY USE ONLY (Leave blank)	2. REPORT DATE	3. REPORT TYPE AND DATES COVERED
	Dec 1990	Master's Thesis

4. TITLE AND SUBTITLE	5 FUNDING NUMBERS
Radar Image Processing for the AFIT Anechoic Chamber	

6. AUTHOR(S)

Brian K. Sanders, Capt USAF

7. PERFORMING ORGANIZATION NAME(S) AND ADDRESS(ES)	8. PERFORMING ORGANIZATION REPORT NUMBER
Air Force Institute of Technology WPAFB OH 45433-6583	AFIT/GE/ENG/90D-54

9. SPONSORING MONITORING AGENCY NAME(S) AND ADDRESS(ES)	10. SPONSORING MONITORING AGENCY REPORT NUMBER

11. SUPPLEMENTARY NOTES

12a DISTRIBUTION AVAILABILITY STATEMENT	12b DISTRIBUTION CODE
Approved for Public Release; Distribution Unlimited	

13. ABSTRACT (Maximum 200 words)

The purpose of this study was to begin development of an Inverse Synthetic Aperture Radar imaging capability for the AFIT anechoic chamber. This began with an evaluation of the capabilities and limitations of the existing radar system and the chamber itself for this application. Then, after deciding on the image processing approach, software had to be written to collect the data necessary for image processing. This constituted the majority of this study, and resulted in a versatile, user-friendly program that automates the process of collecting data for high-resolution radar images. The program checks that the data to be collected will lead to a valid radar cross-section (RCS) image, but will allow data collection for general radar images. Finally, the image processing software was begun. This made use of commercially available software packages called PC-MATLAB and PRO-MATLAB. Further work is needed on the image processing software to generate calibrated images, and to perform image focusing.

14. SUBJECT TERMS		15 NUMBER OF PAGES
Radar Imaging, Synthetic Aperture Radar, Inverse Synthetic Aperture Radar, Image Processing		100
		16 PRICE CODE

17. SECURITY CLASSIFICATION OF REPORT	18 SECURITY CLASSIFICATION OF THIS PAGE	19. SECURITY CLASSIFICATION OF ABSTRACT	20. LIMITATION OF ABSTRACT
Unclassified	Unclassified	Unclassified	UL